

WNK1-regulated inhibitory phosphorylation of the KCC2 cotransporter maintains the depolarizing action of GABA in immature neurons

Perrine Friedel,^{1,2*†} Kristopher T. Kahle,^{3*‡} Jinwei Zhang,^{4*} Nicholas Hertz,⁵
Lucie I. Pisella,^{1,2} Emmanuelle Buhler,^{2,6} Fabienne Schaller,^{2,6} JingJing Duan,³
Arjun R. Khanna,³ Paul N. Bishop,⁷ Kevan M. Shokat,⁵ Igor Medina^{1,2‡}

Activation of Cl⁻-permeable γ -aminobutyric acid type A (GABA_A) receptors elicits synaptic inhibition in mature neurons but excitation in immature neurons. This developmental “switch” in the GABA function depends on a postnatal decrease in intraneuronal Cl⁻ concentration mediated by KCC2, a Cl⁻-extruding K⁺-Cl⁻ cotransporter. We showed that the serine-threonine kinase WNK1 [with no lysine (K)] forms a physical complex with KCC2 in the developing mouse brain. Dominant-negative mutation, genetic depletion, or chemical inhibition of WNK1 in immature neurons triggered a hyperpolarizing shift in GABA activity by enhancing KCC2-mediated Cl⁻ extrusion. This increase in KCC2 activity resulted from reduced inhibitory phosphorylation of KCC2 at two C-terminal threonines, Thr⁹⁰⁶ and Thr¹⁰⁰⁷. Phosphorylation of both Thr⁹⁰⁶ and Thr¹⁰⁰⁷ was increased in immature versus mature neurons. Together, these data provide insight into the mechanism regulating Cl⁻ homeostasis in immature neurons, and suggest that WNK1-regulated changes in KCC2 phosphorylation contribute to the developmental excitatory-to-inhibitory GABA sequence.

INTRODUCTION

Intracellular Cl⁻ concentration [Cl⁻]_i is precisely regulated to maintain cell volume (1), drive transepithelial transport (2), and modulate neuronal excitability (3). Mechanisms that sense alterations in [Cl⁻]_i and transduce these signals to plasmalemmal Cl⁻-transporting proteins are critical to maintain Cl⁻ homeostasis and are required for cell and organismal survival (4). Although the molecular identities of the proteins mediating Cl⁻ transport, which include channels, transporters, and exchangers, are now largely known (5), the molecules and pathways that regulate them to establish context-specific activity are incompletely characterized.

Human and mouse genetics have unequivocally demonstrated that the *SLC12A* family that encodes cation-Cl⁻ cotransporters (CCCs)—the Cl⁻-intruding Na⁺-K⁺-2Cl⁻ cotransporters (NKCCs) and the Cl⁻-extruding K⁺-Cl⁻ cotransporters (KCCs)—are primary determinants of [Cl⁻]_i in multiple cell types (2, 3, 6). The WNK [with no lysine (K)] and SPAK (SPS1-related proline/alanine-rich kinase) serine-threonine kinase cascade is a critical regulator of these Cl⁻ transporters across evolution (7). Although WNK-SPAK kinase signaling has been extensively characterized in epithelial tissues active in water and solute transport such as the kidney's distal

nephron (8–11), the role of this pathway in the central nervous system (CNS) is not well understood.

The emergence of inhibitory GABAergic signaling in the developing CNS demonstrates how changes in [Cl⁻]_i can modulate γ -aminobutyric acid (GABA) activity and, consequently, the function of neurons and circuits. GABA type A receptors (GABA_ARs) are ligand-gated, Cl⁻-permeable ion channels that allow the bidirectional flux of Cl⁻ ions, the direction of which is dictated by [Cl⁻]_i and the membrane potential (12). In the adult brain, GABA_AR activation triggers membrane hyperpolarization and synaptic inhibition. Conversely, in the developing brain, GABA_AR activation triggers depolarization and, in some instances, excitation. This depolarizing activity of GABAergic signaling is critical for neuronal proliferation and migration and synaptogenesis (13). This developmental “switch” in GABA function from excitatory to inhibitory has been attributed to a difference in the [Cl⁻]_i of immature (15 to 20 mM) versus mature neurons (~4 mM), which results from a KCC2-dependent increase in neuronal Cl⁻ extrusion beginning in the first week after birth in mice and rats (14).

The abundance of KCC2 increases during development in some neuronal populations (15), but it is unclear if changes in abundance alone or changes in the functional regulation of the transporter explain the overall increase in KCC2 activity (16). In the hippocampi and cortices of both rats and mice, KCC2 appears in late embryonic stages, and its abundance increases progressively during the first postnatal week (14, 15, 17, 18). However, the first signs of KCC2 function are not detectable until postnatal day 5 (P5) to P6 in the hippocampi and days 6 to 8 in the cortex (15, 18–20), and GABA remains depolarizing until P8 to P13 (21, 22). Discordance between the amount of KCC2 and KCC2 activity has also been reported in cultured immature hippocampal neurons (19). Together, these data suggest that other regulatory factors may contribute to maintaining low KCC2 activity in immature neurons in the developing brain. Phosphorylation of KCC2 alters its activity, as well as affects neuronal [Cl⁻]_i and the GABA reversal potential (E_{GABA}) (16, 23–26). KCC2 phosphorylation

¹Institut de Neurobiologie de la Méditerranée (INMED), INSERM Unité 901, 13273 Marseille, France. ²Aix-Marseille Université, UMR 901, 13273 Marseille, France. ³Department of Neurosurgery, Boston Children's Hospital and Harvard Medical School, Boston, MA 02115, USA. ⁴UK Medical Research Council Protein Phosphorylation and Ubiquitylation Unit, College of Life Sciences, University of Dundee, Dundee DD1 5EH, UK. ⁵Howard Hughes Medical Institute and Department of Cellular and Molecular Pharmacology, University of California San Francisco, San Francisco, CA 94143-0450, USA. ⁶Plateforme Post-Génomique, INMED, 13273 Marseille, France. ⁷School of Biochemistry, University of Bristol, Bristol BS8 1TH, UK.

*These authors contributed equally to this work.

†Present address: Department of Cellular and Molecular Physiology, Yale School of Medicine, New Haven, CT 06520, USA.

‡Corresponding author. E-mail: kkahle@enders.tch.harvard.edu (K.T.K.); igor.medyna@inserm.fr (I.M.)

at Thr⁹⁰⁶ is relatively high in immature brain and decreases progressively during neuronal development (16).

The Cl⁻-sensitive (27) WNK kinases regulate the phosphorylation state and the associated activity of the CCCs either directly or through activation of SPAK or the related oxidative stress-responsive 1 protein (OSR1) kinases (7, 28). Mutations in genes that encode proteins mediating the proteolytic degradation of the WNKs (CUL3 and KLCH3) (29), WNKs themselves (WNK1 and WNK4) (30), or WNK targets [NCC (Na⁺-Cl⁻-cotransporter) and NKCC2, which are kidney-specific CCCs] (31) occur in Mendelian forms of renal electrolyte imbalance and blood pressure dysregulation because of dysregulated Cl⁻ reabsorption (along with Na⁺ or K⁺ or both) in the nephron of the kidney (7). However, WNKs, including WNK2 and WNK3, are abundant in other tissues, including the developing and mature CNS (32–34). Furthermore, *WNK1*, *WNK2*, and *WNK3* each encode multiple isoforms, some of which exhibit remarkable specificity in the brain or spinal cord (35, 36). Mutations in the hereditary sensory neuropathy type II (HSN2) isoform of WNK1, an isoform that is particularly abundant in the CNS, cause a severe autosomal recessive disease in humans characterized by congenital insensitivity to pain [Online Mendelian Inheritance in Man (OMIM) #201300 (35)], suggesting an important role for the WNK kinases in the human CNS. *WNK1* transcripts are expressed in the developing CNS, including the CA1, CA2, and CA3 areas of the hippocampus (36).

Given the presence of WNK kinases in the CNS, their role in regulating the CCCs in other tissues and the CNS of lower organisms (37), and the conservation of phosphoregulatory mechanisms of all CCC family members (7), WNKs are compelling candidate regulators of neuronal Cl⁻ homeostasis through KCC2. WNKs inhibit heterologously expressed KCCs in oocytes, and inhibition of WNKs leads to activation of KCCs (33); WNK1 is required for KCC3 phosphorylation in human embryonic kidney 293 (HEK293) cells (16); and WNK1 kinase activity is regulated by changes in [Cl⁻]_i (27). Therefore, we hypothesized that WNK1 functioned in the developing brain to limit KCC2 activity and maintain GABAergic signaling as excitatory until the developmental switch.

We determined that knocking down WNK1 or pharmacological inhibition of WNK1 significantly enhanced KCC2-dependent Cl⁻ extrusion, lowered [Cl⁻]_i, and caused an ~15-mV hyperpolarizing shift of the E_{GABA} . Our data suggested that WNK1 complements other mechanisms that regulate gene expression (14) and contributes to the depolarizing action of GABA in immature neurons by promoting the inhibitory phosphorylation of KCC2 at Thr⁹⁰⁶ and Thr¹⁰⁰⁷.

RESULTS

WNK1 kinase inhibition facilitates KCC2-dependent Cl⁻ extrusion and causes a hyperpolarizing shift in E_{GABA} in immature neurons

To test whether WNK1 regulates KCC2-dependent neuronal Cl⁻ homeostasis, we expressed constitutively active (S382E) or kinase-dead, dominant-negative (D368A) WNK1 mutants (24) (herein termed “WNK1-CA” and “WNK1-DN”, respectively) in cultured hippocampal neurons of different days in vitro (div) and measured the E_{GABA} and calculated [Cl⁻]_i from gramicidin-perforated patch-clamp recordings (see Materials and Methods) (Fig. 1A). Because WNK1 can also regulate the activity of the Cl⁻ intruder NKCC1 (38), which is present in neurons (3), all measurements of E_{GABA} were performed in the presence of bumetanide, which is a relatively specific inhibitor of NKCC1 at low concentrations (10 μM). In our preparations of cultured hippocampal neurons, 10 μM bumetanide produced a 5-mV negative shift of E_{GABA} in immature neurons

(6 to 7 div) and an 8-mV negative shift in more mature cells (13 to 15 div) (Fig. 1B).

In immature neurons (6 to 7 div), genetic silencing of WNK1 using specific short hairpin RNAs (shRNAs) (fig. S1) or expression of WNK1-DN produced a significant ~15-mV hyperpolarizing shift of E_{GABA} (Fig. 1C, columns 1 to 3). The effect of WNK1 shRNA was specific because E_{GABA} was similar to control when the WNK1 was rescued by the expression of an shRNA-resistant WNK1-CA mutant (Fig. 1C, column 4). Critically, the hyperpolarizing shift of E_{GABA} associated with WNK1 knockdown depended on KCC2 because neurons coexpressing WNK1 and KCC2 shRNAs failed to elicit a hyperpolarizing shift in E_{GABA} (Fig. 1C, column 5).

Conversely, E_{GABA} was similar in control immature neurons transfected with scrambled shRNA and in neurons expressing WNK1-CA (Fig. 1C, columns 1 and 6) and was also similar to those recorded from immature neurons in which KCC2 was knocked down (Fig. 1C, column 7). These results showed that loss of WNK1 activity in immature neurons elicited a KCC2-dependent hyperpolarizing shift of E_{GABA} , whereas constitutive WNK1 activation had no detectable effect.

In more mature neurons (13 to 15 div), which were characterized by significantly more hyperpolarized E_{GABA} values [-83.1 ± 1.7 mV ($n = 9$) in the 13 to 15 div neurons compared to 57.9 ± 1.5 mV ($n = 14$) in the 6 to 7 div neurons], the expression of WNK1 shRNA or WNK1-DN did not elicit further hyperpolarization of E_{GABA} (Fig. 1C, columns 1 to 3). Conversely, mature neurons (13 to 15 div) expressing WNK1-CA exhibited a depolarizing shift of E_{GABA} (Fig. 1C, column 6); these values were, however, more significantly negative than those measured in neurons in which KCC2 was knocked down (Fig. 1C, column 7).

We also measured the recovery to baseline of GABA_AR-mediated currents (I_{GABAA}) in immature neurons that had been preloaded with Cl⁻ (see Materials and Methods). This experiment provides an indication of the rate of Cl⁻ extrusion (39). The I_{GABAA} were induced by brief focal applications of isoguvacine, a GABA_AR agonist, at a holding potential (V_h) of -80 mV, whereas Cl⁻ loading was obtained using the combination of a 10-s isoguvacine pulse and neuron depolarization to -20 mV. Consistent with a potentiating effect of WNK1 knockdown on Cl⁻ extrusion, neurons expressing WNK1 shRNA exhibited a shortened time of GABA_AR test response recovery after Cl⁻ loading, an effect rescued by the expression of shRNA-resistant WNK1-CA (Fig. 1, D and E). These experiments suggested that endogenous WNK1 contributes to the KCC2-dependent control of Cl⁻ homeostasis in immature (6 to 7 div), but not in more mature (13 to 15 div), cultured hippocampal neurons.

In utero inhibition of WNK1 lowers neuronal [Cl⁻]_i and causes a hyperpolarizing shift in GABA activity

To determine if the findings from the cultured neurons are relevant in vivo, we studied whether WNK1 knockdown in immature neurons in utero affects [Cl⁻]_i and GABA activity. We used the genetically encoded biosensor of Cl⁻, Cl-Sensor, to monitor changes in [Cl⁻]_i (40). Constructs encoding Cl-Sensor plus scrambled shRNA (control) or Cl-Sensor plus WNK1 shRNA were electroporated in utero in rats at E15 (see Materials and Methods). We prepared transverse slices of cortex on P3 to P5 and P30. Electroporated slices contained hundreds of neurons expressing Cl-Sensor in cortical layers III to V (Fig. 2A), which exhibited variable fluorescence ratio signals obtained using excitation at 430 and 500 nm ($R_{430/500}$) (Fig. 2B); however, the basal mean fluorescence ratio measured before application of isoguvacine was similar between the scrambled shRNA control and the WNK1 shRNA animals (Fig. 2C). The absolute mean values of $R_{430/500}$ were higher in immature than in mature slices (Fig. 2B), which is in agreement with the developmental profile of the resting neuronal [Cl⁻]_i.

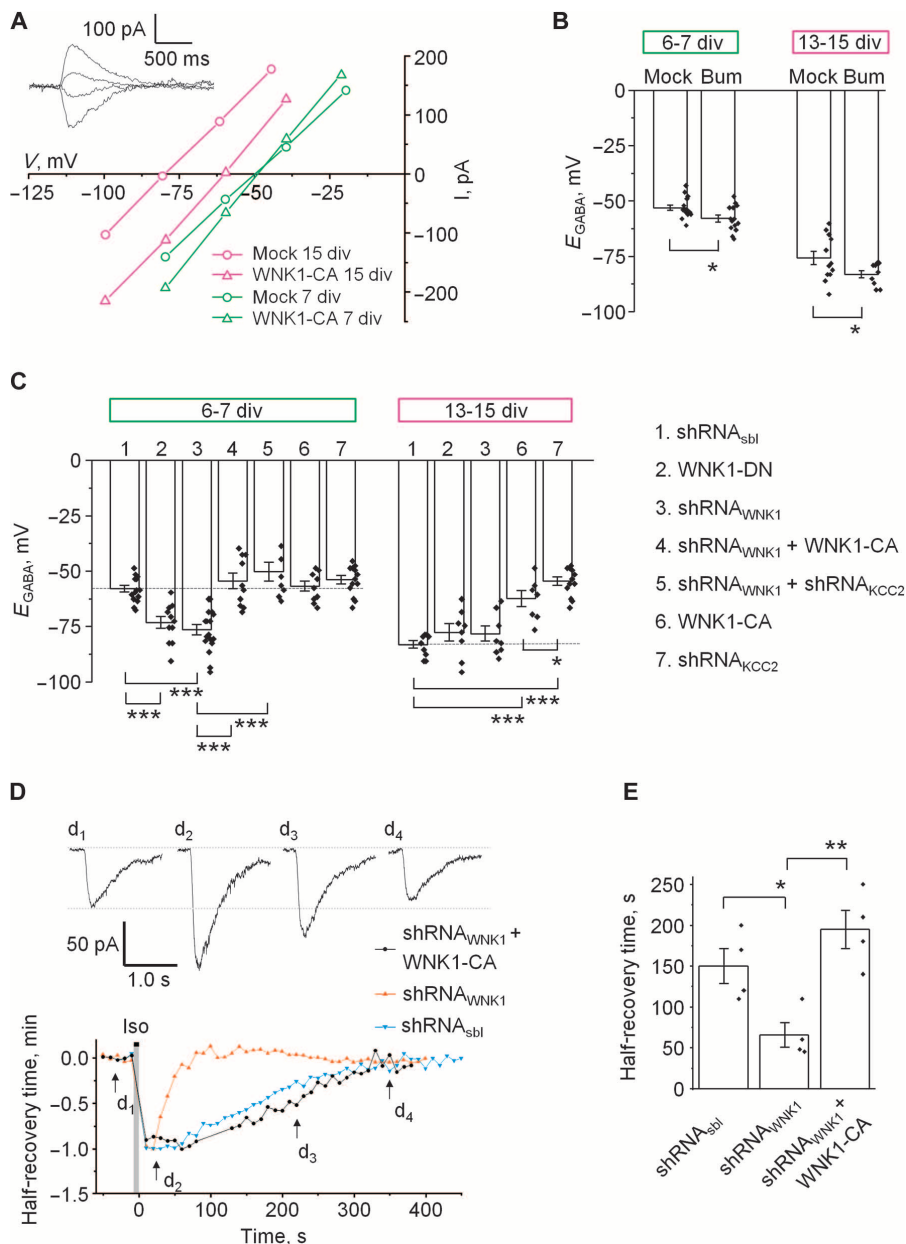


Fig. 1. WNK1-dependent regulation of E_{GABA} in immature, but not in mature, cultured hippocampal neurons. (A) Typical gramicidin-perforated patch-clamp recordings of $GABA_A$ -mediated currents (I) induced by short (50 ms) focal application of isoguvacine (iso) at different membrane potentials (focal I_{GABAA}). E_{GABA} was determined as the intercept of the I - V curve with the x axis. Inset traces illustrate I_{GABAA} recorded from 7 div neurons expressing WNK1-CA. (B) Bar graph illustrating the mean \pm SEM of E_{GABA} in neurons of different ages transfected with enhanced green fluorescent protein (eGFP) and scrambled shRNA and recorded with or without bumetanide (Bum; 10 μ M). * P < 0.05, analysis of variance (ANOVA) test. Data represented are pooled from five separate experiments, with one to three neurons per experiment. (C) E_{GABA} in neurons of different ages transfected with eGFP and the constructs indicated in the key (1 to 7). Data represented are pooled from four to five experiments for each construct, with one to three neurons per experiment. *** P < 0.001, ANOVA test. (D) Examples of focal I_{GABAA} recorded at V_h of -80 mV before and after neuronal Cl^- loading achieved using combination of a 10-s isoguvacine pulse and neuron depolarization to -20 mV. The kinetics of the recovery reflect neuronal Cl^- clearance. d_1 to d_4 are traces of I_{GABAA} recorded from neuron expressing $shRNA_{WNK1} + WNK1-CA$ at different times of experiment as indicated with arrows on the plot. (E) Mean \pm SEM half-time of I_{GABAA} recovery in neurons expressing indicated constructs. * P < 0.05; ** P < 0.01, ANOVA test.

Measurement of the exact $[Cl^-]_i$ is not possible with Cl^- Sensor because of its sensitivity to H^+ and some organic ions; however, Cl^- Sensor can be used to detect weak (2 to 4 mM) oscillations of resting $[Cl^-]_i$ (for example, in response to $GABA_A$ or glycine receptor activation) (40). Thus, Cl^- Sensor is suitable for measurements of neuronal Cl^- extrusion capacity. We therefore avoided using ratiometric Cl^- Sensor recordings to measure $[Cl^-]_i$ or the magnitude of $[Cl^-]_i$ changes. Instead, we designed all experiments to determine the directionality of Cl^- -dependent fluorescence changes in response to $GABA_A$ activation, thereby we could evaluate the relative difference in $[Cl^-]_i$ inside the neuron and in the medium.

Consistent with the age-dependent depolarizing and hyperpolarizing actions of GABA in immature and mature neurons, respectively (41), brief exposure of brain slices from control mice (animals electroporated with Cl^- Sensor and scrambled shRNA) to isoguvacine (30 μ M, 3 min) produced distinct fluorescence responses dependent on the age of the animal. In slices from immature P3 to P5 mice, most of the neurons (80%) exhibited a uniform decrease in $R_{430/500}$ [indicated by an arrow in Fig. 2B (top) and by the negative value of $\Delta R/R$ in Fig. 2D], reflecting an outward direction of Cl^- flux characteristic of GABA depolarizing activity. In slices from more mature (P30) animals, similar isoguvacine applications elicited no change ($\sim 60\%$ of neurons) or an increase in $R_{430/500}$ [indicated by an arrow in Fig. 2B (bottom) and by the positive value of $\Delta R/R$ in Fig. 2D], reflecting either Cl^- equilibrium or Cl^- influx, typical for GABA hyperpolarizing activity.

To test whether WNK1 knockdown affects Cl^- extrusion efficacy in this model, we applied artificial cerebrospinal fluid (ACSF) solution containing 25 mM KCl (to depolarize neurons) and 30 μ M isoguvacine (to load neurons with Cl^- by $GABA_A$ activation) in P3 to P5 and P30 slice preparations. This protocol produced a robust increase in $R_{430/500}$, reflecting a rise in neuronal $[Cl^-]_i$ that recovered progressively to the control values after isoguvacine wash-out (Fig. 2B). However, in immature P3 to P5 slices expressing WNK1 shRNA, the half-recovery time was significantly shorter than those measured in slices expressing scrambled control shRNA (Fig. 2E, top). In contrast, WNK1 knockdown did not affect the half-recovery time of the fluorescence after imposed Cl^- overload in P30 slices (Fig. 2E, bottom). These results suggested

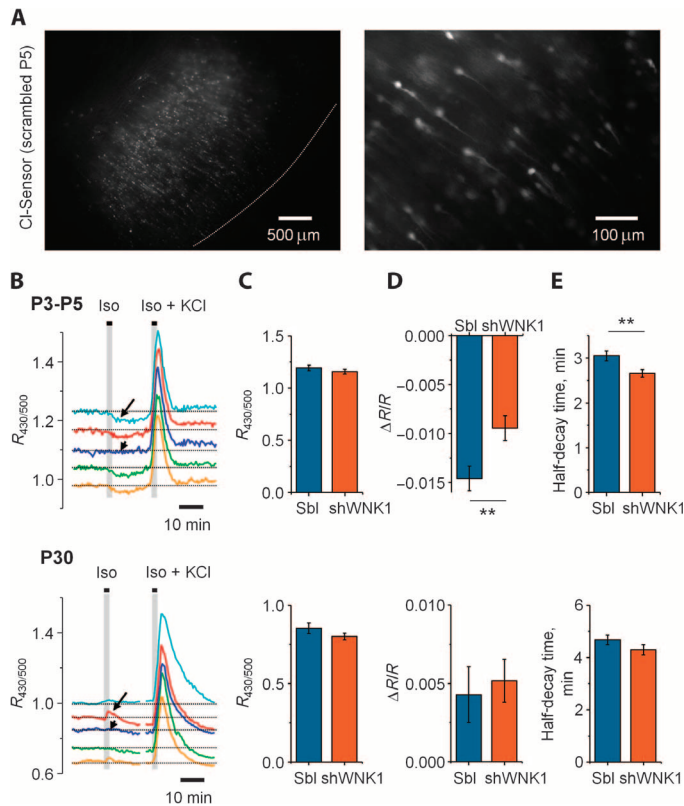


Fig. 2. WNK1-dependent regulation of Cl-Sensor ratiometric fluorescence in acute cortical slices prepared from rats on P3 to P5 and P30. Rats were electroporated in utero at embryonic day 15 with Cl-Sensor plus scrambled shRNA (Sbl) or shRNA_{WNK1} (shWNK1). Data represent results obtained from five rats per experimental condition. Two to three slices were recorded per animal. (A) Typical images of Cl-Sensor fluorescence excited at 500 nm and taken at different optical magnifications in slice from P5 rat electroporated with Cl-Sensor and scrambled shRNA. The dotted white line indicates the slice border. The region of interest was drawn around the soma of cells located in the focal plane. (B) Typical ratiometric fluorescence ($R_{430/500}$) recordings from different neurons (encoded by different colors). Vertical bars indicate the times of application of ACSF containing iso or iso + 25 mM KCl. Arrows and arrowheads indicate different types of responses. Top, P3 to P5; bottom, P30. (C) Mean \pm SEM of basal levels of $R_{430/500}$ measured before iso application. Top, P3 to P5; bottom, P30. Differences are not significantly different at both ages, ANOVA test; $n = 5$. (D) Bar graphs illustrating the mean \pm SEM of fluorescence change $\Delta R/R$, where R is the mean of five measurements before iso application and ΔR is the difference between absolute maximum of iso-induced response and R . $**P < 0.01$, ANOVA test; $n = 5$. Top, P3 to P5; bottom, P30. (E) Half-decay times of the fluorescence recovery after neuronal loading with Cl^- . $**P < 0.01$, ANOVA test; $n = 5$. Top, P3 to P5; bottom, P30.

that in utero WNK1 knockdown facilitates KCC2-dependent neuronal Cl^- extrusion and causes a hyperpolarizing shift in GABA activity only in the immature neurons.

The $R_{430/500}$ half-recovery times after Cl^- overload measured in immature slices were unexpectedly faster than those measured in more mature slices (3.1 ± 0.1 min versus 4.6 ± 0.2 min, $P < 0.01$; Fig. 2E).

The reason for the slower fluorescence recovery times observed in mature slices is unclear. We hypothesize that the tissue in mature slices is denser and, therefore, the time of KCl washout from the extracellular space is longer. Consequently, residual KCl in extracellular space could maintain KCC2 in reverse or close-to-zero transport mode (42) and, thus, slow Cl^- extrusion. Because the main purpose of our study was to compare Cl^- extrusion between two sets of slices from the same littermate animals, the different age-dependent kinetics of Cl^- recovery are not critical for the given study, but certainly will be a subject of future detailed investigations.

KCC2 is significantly more phosphorylated at Thr⁹⁰⁶ and Thr¹⁰⁰⁷ in immature versus mature neurons

When overexpressed in HEK293 cells, KCC2 is robustly phosphorylated at Thr⁹⁰⁶ and Thr¹⁰⁰⁷, two key regulatory residues, and dephosphorylation of these sites significantly stimulates KCC2 activity (16, 26). KCC2 is significantly more phosphorylated at Thr⁹⁰⁶ in the immature whole mouse brain versus the adult brain, and this temporal difference parallels the developmental increase in KCC2 activity (16). We hypothesized that WNK1 regulates KCC2 phosphorylation at either Thr⁹⁰⁶ or Thr¹⁰⁰⁷, or at both sites, in immature neurons, and that WNK1 antagonism would stimulate KCC2 activity by reducing its phosphorylation at these sites.

To investigate whether either or both residues were phosphorylated, we assayed KCC2 in dissociated rat hippocampal and cortical neurons grown in vitro for 6 to 7 or 14 to 15 days under the same conditions used for physiological experiments and detected KCC2 by Western blot and Thr⁹⁰⁶ and Thr¹⁰⁰⁷ phosphorylation by immunoprecipitation with phosphorylation site-specific antibodies (26). The abundance of KCC2 increased in more mature neurons (Fig. 3A). However, the relative amount of KCC2 phosphorylated at both Thr⁹⁰⁶ and Thr¹⁰⁰⁷ was significantly increased in KCC2 immunoprecipitated from 6 to 7 div neurons compared to that isolated from 14 to 15 div neurons (Fig. 3A and fig. S2).

We predicted that WNK1, SPAK, and OSR1 would be more active in the 7 div cultures that exhibited increased relative phosphorylation of KCC2. Therefore, we measured the total amount and phosphorylation status of WNK1 and SPAK at residues required for the activation of these enzymes (26) in the same cultures (Fig. 3B). The relative amounts of phosphorylated WNK1 at Ser³⁸², SPAK at Ser³⁷³, and OSR1 at Ser³²⁵ were also significantly increased in 6 to 7 div neurons compared to those in 14 to 15 div neurons. These results showed that KCC2 Thr⁹⁰⁶ and Thr¹⁰⁰⁷ phosphorylation and phosphorylation events associated with WNK1 pathway activation are increased in immature neurons relative to mature neurons.

Alteration of KCC2 Thr⁹⁰⁶ and Thr¹⁰⁰⁷ phosphorylation modulates KCC2 function and GABA activity

Does modulation of KCC2 Thr⁹⁰⁶ and Thr¹⁰⁰⁷ phosphorylation affect KCC2 activity in immature neurons? Mutations mimicking KCC2 phosphorylation at Thr⁹⁰⁶ and Thr¹⁰⁰⁷ (T906E/T1007E) partially inhibit KCC2 activity when expressed in HEK293 cells (16, 26) and neuronal cells electroporated in utero (24), whereas mutations mimicking a dephosphorylated state (T906A/T1007A) activate KCC2 (16, 24, 26). We validated that genetic mutation preventing or mimicking KCC2 phosphorylation at these sites alters KCC2 activity in cultured hippocampal neurons. We engineered nonphosphorylatable T906A/T1007A (KCC2^{A/A}) and phosphomimetic T906E/T1007E (KCC2^{E/E}) KCC2 mutants in an shRNA-resistant KCC2 expression plasmid enabling production of KCC2 mutant protein in the context of endogenous KCC2 depletion, achieved with a previously characterized shRNA designed to target rat KCC2 (39). As in previous experiments (39), knockdown of KCC2 produced a depolarizing shift in E_{GABA} in 10 div cultured rat hippocampal neurons (Fig. 4A, compare nontransfected or shRNA_{sbl} with mock shRNA_{KCC2}). Expression of KCC2^{A/A} in

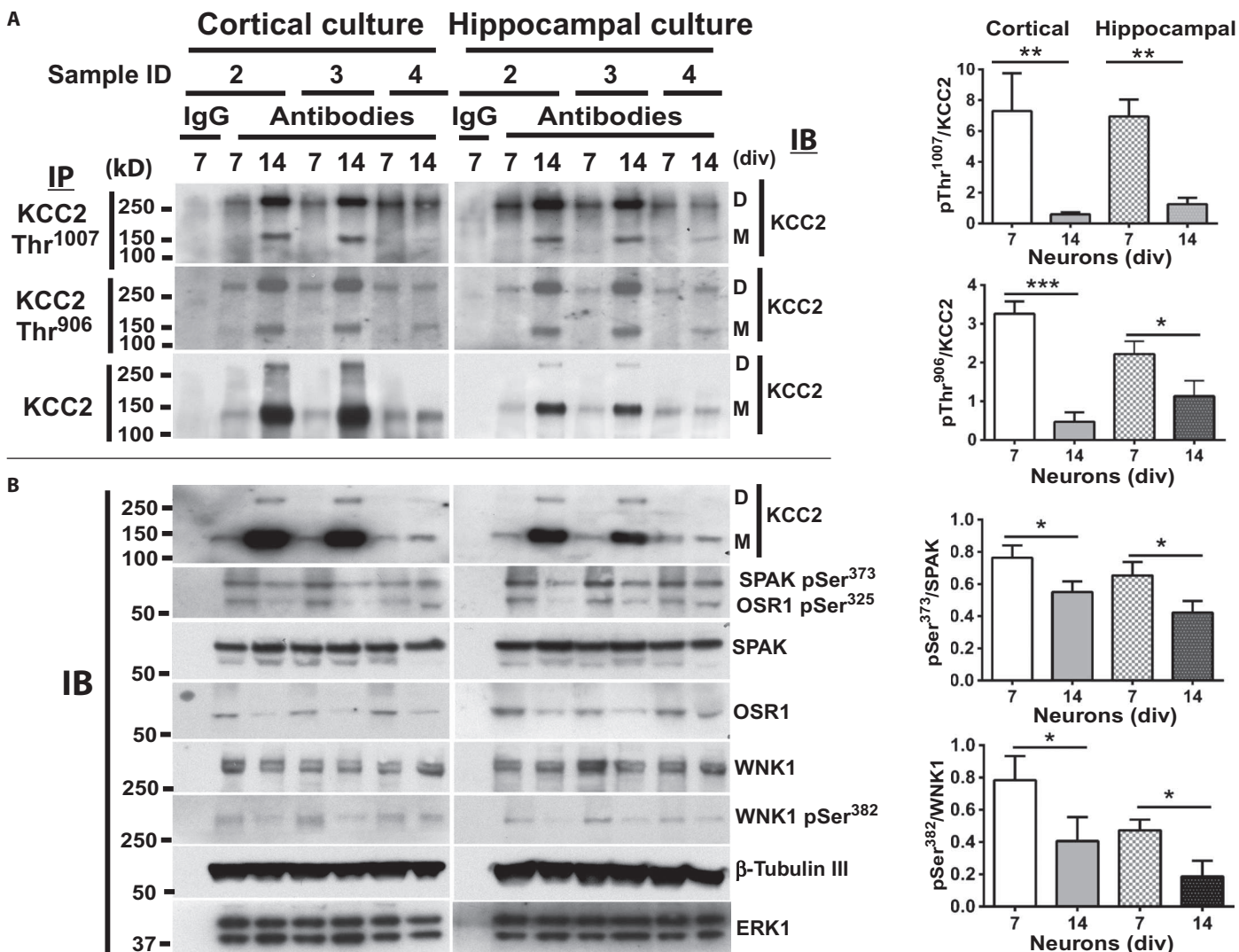


Fig. 3. WNK-SPAK/OSR1 regulation and phosphorylation of endogenous KCC2 in immature and mature cultured hippocampal and cortical neurons. (A) Neuronal lysates were subjected to immunoprecipitation (IP) with the indicated pan-KCC2 antibody (KCC2) or phosphorylation site-specific antibodies recognizing the Thr⁹⁰⁶- or Thr¹⁰⁰⁷-phosphorylated forms (IP), and protein was detected with the pan-KCC2 antibody (IB). Band intensities were quantified using ImageJ software. Right panel shows the quantification (ratio calculation) based on (phospho-dimeric KCC2 + phospho-monomeric KCC2)/(total dimeric KCC2 + monomeric KCC2). ****P* < 0.001; ***P* < 0.01; **P* < 0.05; ns, nonsignificant (unpaired *t* test; *n* = 3; error

bars represent mean ± SEM). (See fig. S2 for details about how bands were selected for quantification.) D, dimeric KCC2; M, monomeric KCC2; ERK1, extracellular signal-regulated kinase. (B) Whole-cell lysates were subjected to immunoblot analysis with antibodies recognizing the indicated proteins or phosphorylated proteins. Data shown are representative of three separate experiments. Band intensities were quantified using ImageJ software. Right panel shows the quantification (ratio calculation) based on (phospho-Ser³⁷³ SPAK/total SPAK) and (phospho-Ser³⁸² WNK1/total WNK1). ****P* < 0.001; ***P* < 0.01; **P* < 0.05; ns, nonsignificant (unpaired *t* test; *n* = 3; error bars represent mean ± SEM).

KCC2-knockdown neurons elicited a -14-mV hyperpolarizing shift of E_{GABA} compared to KCC2-knockdown neurons expressing KCC2^{E/E} (Fig. 4A). Although the hyperpolarizing shift produced by expression of KCC2^{E/E} was less than that produced by expression of KCC2^{A/A}, KCC2^{E/E} still triggered a significant hyperpolarizing shift of E_{GABA} relative to KCC2-knockdown neurons, suggesting that T906E/T1007E phosphorylation decreases but does not eliminate transporter activity, consistent with previous reports (16, 24). KCC2-knockdown neurons expressing shRNA-resistant wild-type KCC2 exhibited an E_{GABA} intermediate between those of neurons expressing KCC2^{E/E} and KCC2^{A/A} (Fig. 4A).

KCC2 Thr⁹⁰⁶ and Thr¹⁰⁰⁷ phosphorylation regulates cotransporter activity by altering its surface abundance

Phosphorylation could affect the intrinsic transport activity of molecules or the transport of functional molecules to or from the cell surface. We assessed the abundance of KCC2, KCC2^{E/E}, or KCC2^{A/A} expressed in different cell compartments of 10 div hippocampal neurons, using a previously described KCC2 construct that contains a tag (pFluorin) in an external loop of KCC2 (KCC2-pH_{ext}) (43) and with a multistep immunolabeling protocol (Fig. 4B). With neurons expressing KCC2-pH_{ext} mutants, we visualized the total amount of KCC2-pH_{ext} [total fluorescence

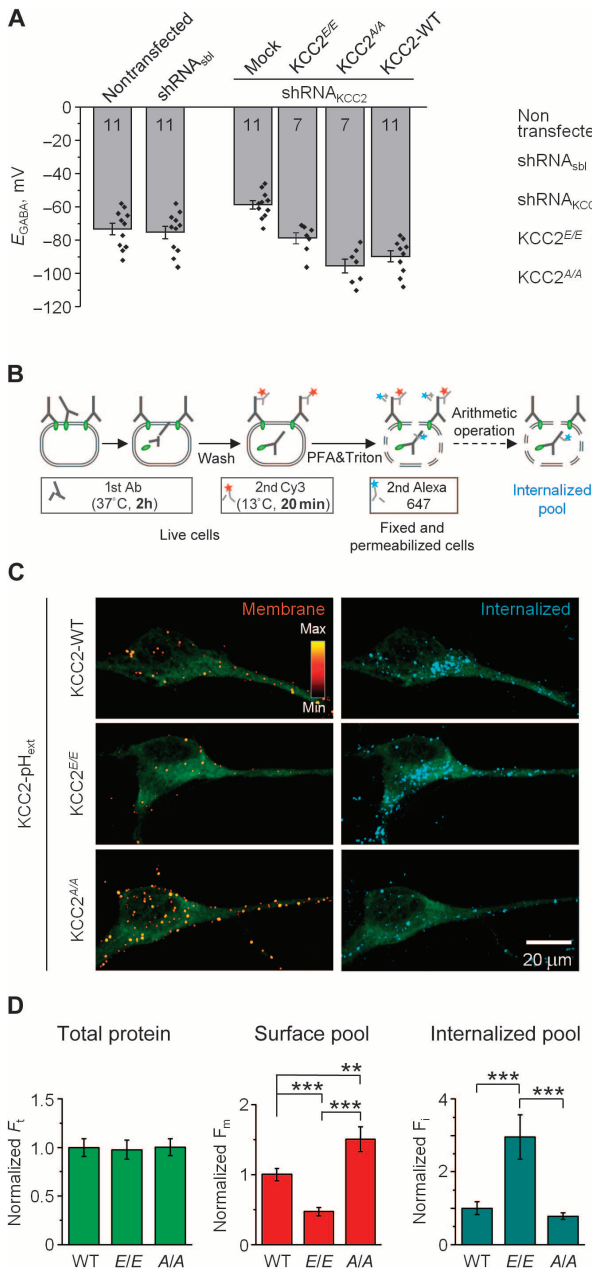


Fig. 4. Genetic modulation of KCC2 Thr⁹⁰⁶ and Thr¹⁰⁰⁷ phosphorylation affects E_{GABA} and the plasmalemmal surface expression of KCC2 in cultured hippocampal neurons. (A) E_{GABA} recorded in 10 div neurons that were transfected at 7 div with constructs as indicated. Recordings were made using gramicidin-perforated patch-clamp, as in Fig. 1A. Numbers in columns indicate the number of neurons recorded. The table shows the statistical differences (P) among the samples (one-way ANOVA test). Data are pooled from five separate experiments, with one to three neurons per experiment. (B) Scheme of the multistep immunolabeling protocol. 1st Ab, primary antibody; 2nd Cy3, Cy3-conjugated secondary antibody; 2nd Alexa 647, Alexa-conjugated secondary antibody; PFA, paraformaldehyde. (C) Representative images illustrating membrane staining (F_m , left column) and internalized fluorescence (F_i , right column) of cultured hippocampal cells expressing wild-type (KCC2-WT) and mutated forms of KCC2 with external tag (KCC2-pH_{ext}) as indicated. Neuronal shape is shown in light green in each image. (D) Normalized mean \pm SEM of total protein, membrane staining (F_m), and internalized fluorescence (F_i) for each KCC2-pH_{ext} construct (pooled data from three cultures; five to eight cells per culture and condition). *** $P < 0.001$; ** $P < 0.01$, ANOVA test.

(F_i), the amount of the transporter present at the cell surface [membrane fluorescence (F_m)], and the amount of transporter internalized in a 2-hour period [internalized fluorescence (F_i)]. Whereas the total amount of KCC2-pH_{ext}, KCC2^{E/E}-pH_{ext}, and KCC2^{A/A}-pH_{ext} mutants was similar (Fig. 4, C and D), the intensity of the pools of the KCC2 Thr⁹⁰⁶ and Thr¹⁰⁰⁷ mutants at the surface differed from that of wild-type KCC2. The phosphomimetic KCC2^{E/E}-pH_{ext} mutant was less abundant at the surface and the nonphosphorylatable KCC2^{A/A}-pH_{ext} mutant was more abundant than wild-type KCC2-pH_{ext}. Analysis of the fluorescence intensities emitted by internalized clusters in neurons expressing KCC2^{E/E}-pH_{ext} revealed a prominent accumulation in the region of soma, whereas there is less of the KCC2^{A/A}-pH_{ext} mutant internalized, and the internalized clusters were

distributed along the length of dendrites (Fig. 4C). Neurons expressing KCC2-pH_{ext} exhibited an intermediate pattern of staining. Overall, the relative F_i signal from KCC2^{E/E}-pH_{ext}-expressing neurons was significantly stronger than that from KCC2^{A/A}-pH_{ext}-expressing neurons (Fig. 4D).

We also examined mouse Neuro2A (N2a) cells, which are immortalized neuronal-like cells that have no detectable endogenous KCC2, by Western blot. We transfected into these cells Cl-Sensor (Fig. 5A, green), mCherry-KCC2, or mCherry-tagged versions of the KCC2 phosphorylation mutants (Fig. 5A, red), along with the $\alpha 1$ subunit of human glycine receptor (GlyR), which is a glycine-activated Cl⁻-permeable channel. The co-application of KCl (to depolarize the cells) and glycine (to produce a massive Cl⁻ influx through GlyR) resulted in a strong increase in the $R_{430/500}$ fluorescence ratio (Fig. 5B). The recovery kinetics of $R_{430/500}$ after the washout of KCl and glycine reflected the activity of the KCC2 as defined previously (40). Compared to cells expressing KCC2^{A/A}, cells expressing KCC2^{E/E} exhibited significantly slower kinetics of $R_{430/500}$ recovery, reflecting a lower Cl⁻ extrusion capacity of the KCC2^{E/E} mutant (Fig. 5, C and D). The Cl⁻ extrusion ability of cells expressing wild-type mCherry-KCC2 was similar to that of KCC2^{E/E} mutant (Fig. 5D). These data indicated that the Cl⁻ extrusion capacity of these N2a cells could be controlled by introduction of KCC2, which makes them a useful model for testing regulation of KCC2.

Inhibition of WNK1 activates KCC2 and decreases KCC2 inhibitory phosphorylation at Thr⁹⁰⁶ and Thr¹⁰⁰⁷

We measured the rate of Cl-Sensor fluorescence recovery as an indicator of Cl⁻ extrusion capacity in N2a cells coexpressing mCherry-KCC2 and WNK1-CA or WNK1-DN. WNK1-CA did not affect the kinetics of fluorescence recovery, suggesting that KCC2 phosphorylation was maximal in these cells at baseline. In contrast, WNK1-DN significantly reduced the half-recovery time of the ratiometric fluorescence (Fig. 5E). Furthermore, the enhanced Cl⁻ extrusion capacity in response to WNK1-DN was absent in cells expressing KCC2^{E/E}. The increase in Cl⁻ extrusion capacity of WNK1-DN depended on KCC2 because the Cl⁻ extrusion capacity was low in control cells and became even lower in cells expressing only WNK1-DN (Fig. 5F). These functional data suggest that WNK1-DN triggers KCC2-mediated Cl⁻ extrusion by preventing the inhibitory phosphorylation of KCC2 at Thr⁹⁰⁶ and Thr¹⁰⁰⁷.

We also used a chemical genetic approach (44, 45) to test whether specific inhibition of WNK1 kinase activity alters the activity and phosphorylation of KCC2 (Fig. 6 and fig. S3). The chemical genetic approach

distributed along the length of dendrites (Fig. 4C). Neurons expressing KCC2-pH_{ext} exhibited an intermediate pattern of staining. Overall, the relative F_i signal from KCC2^{E/E}-pH_{ext}-expressing neurons was significantly stronger than that from KCC2^{A/A}-pH_{ext}-expressing neurons (Fig. 4D).

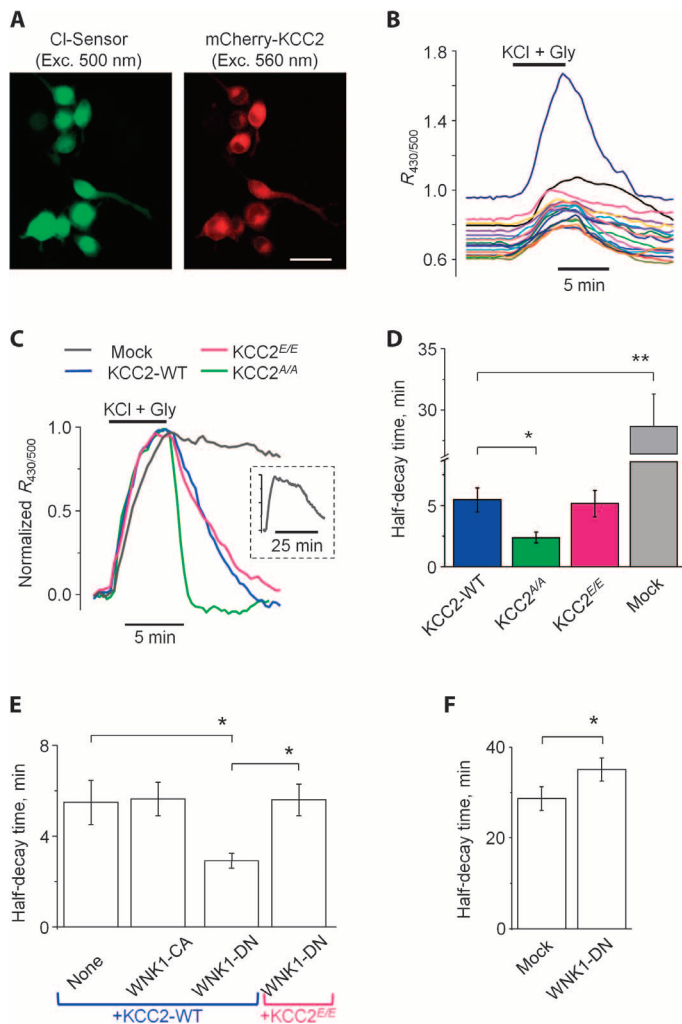


Fig. 5. Phosphomimetic and nonphosphorylatable KCC2 Thr⁹⁰⁶/Thr¹⁰⁰⁷ mutants exhibit different Cl⁻ extrusion capacities and sensitivity to dominant-negative WNK1. (A) Fluorescence signals recorded from N2a cells cotransfected with Cl-Sensor (green), GlyR (nonfluorescent), and mCherry-KCC2 (red). Scale bar, 20 μ m. Excitation wavelength is indicated. (B) Individual traces of Cl-Sensor fluorescence ratio changes measured in N2a cells expressing KCC2^{E/E}. Horizontal bar indicates the time of application of 100 mM KCl and 50 μ M glycine (Gly) to load cells with Cl⁻. The ordinate axis indicates the ratio of Cl-Sensor fluorescence measured at 430- and 500-nm excitation wavelengths ($R_{430/500}$). Different colored lines represent different cells. (C) Normalized mean traces of Cl-Sensor ratiometric fluorescence change in N2a cells expressing the indicated KCC2 constructs. The inset illustrates a full record of $R_{430/500}$ fluorescence from mock-transfected cells shown in the main plot. (D to F) Mean \pm SEM of the half-decay time of Cl⁻ extrusion after glycine + KCl application in cells expressing different combinations of constructs as indicated. $n = 4$ to 5 experiments. ** $P < 0.01$; * $P < 0.05$, ANOVA test.

combines a genetic change, in which a kinase of interest can be mutated to generate a unique binding pocket for adenosine triphosphate (ATP) analogs, and a pair of chemicals in the form of ATP analogs that sensitize the modified kinase to inhibitors that do not affect wild-type kinases. We created an analog-sensitive mutant of WNK1 (WNK1-AS) (fig. S3A) in

which the “gatekeeper” amino acid residue (a large, conserved hydrophobic residue that lines the ATP binding site; T³⁰¹ in WNK1) was replaced by a smaller amino acid (here, alanine). This enlarged the ATP-binding pocket, enabling the binding and utilization of ATP analogs modified with bulky substitutions [here, *N*⁶-benzyl-adenosine 5'-*O*-(3-thiotriphosphate) (*N*⁶-benzyl-ATP- γ -S)], and rendered the kinase susceptible to inhibition by cell-permeable derivatives of the Src inhibitor protein phosphatase 1 (PP1) [here, 1-(1,1-dimethylethyl)-3-(1-naphthalenyl)-PP1 (1-NA-PP1)] with high affinity and selectivity (44–46) (see Materials and Methods).

WNK1-AS utilized *N*⁶-benzyl-ATP- γ -S with much greater efficiency than WNK1-CA in autophosphorylation reactions (fig. S3B) and catalyzed the transfer of benzyl-ATP- γ -S to a known WNK1 substrate, OSR1 (fig. S3C), but failed to transfer benzyl-ATP- γ -S to KCC2 directly (fig. S3C), suggesting that WNK1 does not directly phosphorylate KCC2. WNK1-AS was also inhibited by 1-NA-PP1 in a dose-dependent manner (fig. S3D).

We exploited the sensitivity of WNK1-AS to inhibition with 1-NA-PP1 to test the effect of inhibiting WNK1 kinase activity on KCC2 function and Thr⁹⁰⁶ and Thr¹⁰⁰⁷ phosphorylation. We transfected N2a cells with WNK1-AS or WNK1-CA and measured KCC2-mediated Cl⁻ extrusion in the presence or absence of 1-NA-PP1. Application of 1-NA-PP1 (10 μ M for 10 min) to cells coexpressing KCC2 and WNK1-CA had no effect on the KCC2-dependent fluorescence recovery after loading with Cl⁻ (Fig. 6, A and B). However, in cells coexpressing KCC2 and WNK1-AS, 1-NA-PP1 produced a robust acceleration of KCC2-dependent fluorescence recovery (Fig. 6, A and B). Similar to experiments with WNK1-DN (Fig. 5F), inhibition of WNK1-AS with 1-NA-PP1 did not affect Cl⁻ extrusion in N2a cells expressing KCC2^{E/E} (Fig. 6, A and B). These experiments showed that chemical inhibition of the kinase activity of WNK1 rapidly (within 10 min) enhanced KCC2 activity, and this effect depended on the dephosphorylation of KCC2 at Thr⁹⁰⁶ and Thr¹⁰⁰⁷.

To test whether WNK1 inhibition alters KCC2 phosphorylation at Thr⁹⁰⁶ and Thr¹⁰⁰⁷, we chemically inhibited WNK1-AS with 1-NA-PP1 in N2a cells coexpressing hemagglutinin (HA)-tagged KCC2 and WNK1-CA or WNK1-AS and individually assessed the phosphorylation status of KCC2 at Thr⁹⁰⁶ and Thr¹⁰⁰⁷ using phosphorylation site-specific antibodies (26) (Fig. 6C). Only in cells expressing WNK1-AS did chemical inhibition of WNK1 activity decrease the phosphorylation of both Thr⁹⁰⁶ and Thr¹⁰⁰⁷ (Fig. 6C). Together, these results showed that WNK1 activity promotes the phosphorylation of KCC2 Thr⁹⁰⁶ and Thr¹⁰⁰⁷, and WNK1 inhibition activates KCC2 by decreasing this phosphorylation.

WNK1 and SPAK form a complex with KCC2 in immature neurons and the developing mouse brain

Although our data indicated that WNK1 inhibited KCC2 activity by promoting phosphorylation at Thr⁹⁰⁶ and Thr¹⁰⁰⁷, the data suggested that WNK1 stimulated KCC2 phosphorylation by another kinase. The kinase SPAK is phosphorylated and thus activated by WNK1 (28). The RFXV motif in the N-terminal region of the KCC2a isoform is a binding site for the kinases SPAK and OSR1; this RFXV motif is also present in WNK1 (47). The KCC2b isoform does not have this SPAK-binding site (RFXV), and there are 40 N-terminal amino acid residues that differ between KCC2a and KCC2b (47). SPAK phosphorylates all KCC isoforms, including KCC2, at the residue homologous to Thr¹⁰⁰⁷ in KCC2, but the kinase that phosphorylates Thr⁹⁰⁶ is unknown (26).

Because WNKs often physically interact with their target CCCs (48), we investigated whether WNK1 associated with KCC2. Coimmunoprecipitation experiments revealed that WNK1, along with SPAK, formed a complex with KCC2 in both immature cultured hippocampal and cortical neurons (Fig. 7A) and the developing mouse brain (Fig. 7B). We also detected the related kinase OSR1, which is recognized by the antibody

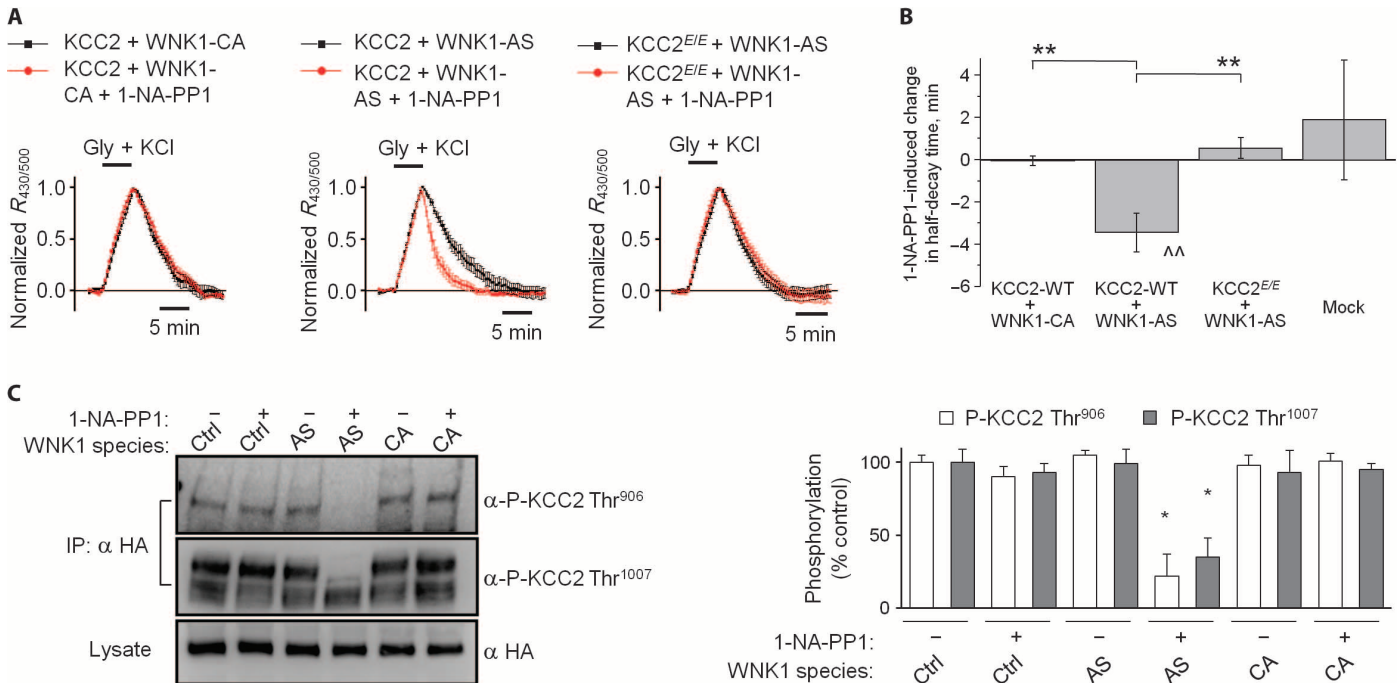


Fig. 6. Chemical genetic inhibition of WNK1 stimulates KCC2 activity. (A) Representative normalized mean \pm SEM traces of the ratiometric Cl-Sensor fluorescence recordings from 8 to 10 N2a cells expressing the indicated combinations of KCC2 and WNK1 in the same experiments before and 10 min after cell incubation with 10 μ M 1-NA-PP1. Horizontal bar indicates the time of application of 100 mM KCl and 50 μ M glycine (Gly) to load cells with Cl⁻. (B) Difference between the half-decay times of Cl⁻ extrusion produced by application of 1-NA-PP1 in cells expressing different combinations of the indicated WNK1 and KCC2 constructs. Mean \pm SEM of four experiments in each series. Two sets of statistical analysis were performed: (i) paired *t* test between half-decay times measured in the same experiments before and 10 min after the beginning of 1-NA-PP1 application. A significant

effect of 1-NA-PP1 was observed only in cells expressing KCC2-WT + WNK1-AS ($^{**}P < 0.01$); (ii) one-way ANOVA test between cells expressing different constructs ($^{**}P < 0.01$). (C) Effect of chemical genetic inhibition of WNK1 kinase activity on KCC2 phosphorylation at Thr⁹⁰⁶ and Thr¹⁰⁰⁷. Myc-tagged WNK1-CA or WNK1-AS was transiently expressed with or without HA-KCC2 in N2a cells in the absence or presence of 1-NA-PP1 (10 μ M for 2 hours). Lysates were harvested and subjected to SDS-polyacrylamide gel electrophoresis (SDS-PAGE), and the phosphorylation at Thr⁹⁰⁶ and Thr¹⁰⁰⁷ was assessed by Western blotting with the antibodies recognizing the indicated proteins or phosphorylated proteins. $^{*}P < 0.01$, significant differences relative to control conditions as assessed by unpaired *t* test ($n = 3$) and ANOVA test. Error bars represent mean \pm SEM.

against SPAK (26), in the WNK1 immunoprecipitates from 7 and 14 div cultures. These results suggested that WNK1 may not only activate SPAK but could also regulate KCC2 Thr⁹⁰⁶ and Thr¹⁰⁰⁷ phosphorylation by serving as a scaffold that bridges SPAK to KCC2 for phosphorylation of Thr¹⁰⁰⁷ and potentially another yet undefined kinase that directly phosphorylates Thr⁹⁰⁶.

DISCUSSION

A paradoxical depolarizing action of GABA due to high [Cl⁻]_i is an evolutionarily conserved hallmark of immature neurons (41) and is related to the delayed postnatal induction of the Cl⁻-extruding KCC2 cotransporter activity (15, 20, 49, 50). The mechanisms underlying the developmental switch in KCC2 activity are not well understood, and it is unclear if changes in the abundance of KCC2 alone or if alterations in transporter regulation also account for the net increase in KCC2 activity. Indeed, previous studies have documented a discrepancy between the amount of KCC2 and the KCC2-dependent Cl⁻ extrusion capacity of immature neurons (15, 19, 20).

Here, we showed that the kinase WNK1 inhibits KCC2 to decrease neuronal Cl⁻ extrusion capacity in immature neurons, thereby contributing to the maintenance of the depolarizing action of GABA (Fig. 8). Our data indicated that the WNK1-dependent inhibitory phosphorylation of KCC2

at Thr⁹⁰⁶ and Thr¹⁰⁰⁷ was the likely mechanism for limiting KCC2 activity. Our results corroborate and extend previous works by Rinehart *et al.* (16), who showed that KCC2 phosphorylation at Thr⁹⁰⁶ inversely correlates with KCC2 activity in the developing mouse brain, and Inoue *et al.* (24), who demonstrated a phosphorylation-dependent inhibitory effect of taurine on KCC2 activity in immature neurons that was recapitulated by WNK1 overexpression in the absence of taurine.

Our model is supported by several corroborating lines of evidence gathered with independent approaches in ex vivo and in vitro systems. Using two complementary methods of WNK1 silencing (dominant-negative overexpression of a kinase-dead WNK1 mutant and shRNA-mediated depletion of endogenous WNK1) and electrophysiological recording (gramicidin-perforated patch), we showed that reduced WNK1 activity shifted *E*_{GABA}, indicative of decreased [Cl⁻]_i, in immature, but not in mature, cultured hippocampal neurons, thereby affecting GABA function. These effects were specific because they were rescued by overexpression of constitutively active WNK1 in the context of endogenous WNK1 depletion and were dependent on KCC2 because they were absent when KCC2 was silenced. Ex vivo experiments with immature rat cortical slices (P3 to P5) supported these in vitro results: In utero WNK1 inhibition prematurely shifted the *E*_{GABA} of immature neurons to less depolarizing values by lowering neuronal [Cl⁻]_i. Chemical genetic inhibition of the kinase activity of WNK1,

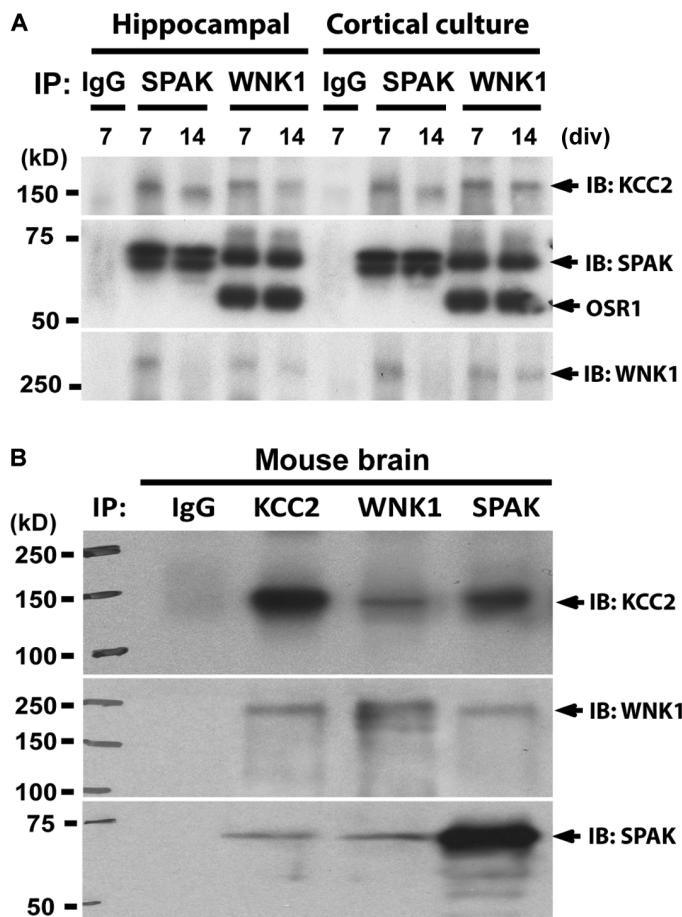


Fig. 7. KCC2 interacts with WNK1 and SPAK in vivo. (A) Lysates from 7 and 14 div hippocampal cultures (sample 2, as indicated in Fig. 3) and cortical cultures (sample 2) were immunoprecipitated (IP) with the indicated WNK1 or SPAK antibodies and analyzed for their interacting partners using standard SDS-PAGE and immunoblotting (IB) techniques. The SPAK antibody also recognizes OSR1 because mammalian SPAK and OSR1 share ~65% amino acid identity and both contain a highly conserved CCT domain that binds WNK1. (B) Whole-brain lysates obtained from P2 mice were immunoprecipitated with the indicated antibodies recognizing WNK1, SPAK, or KCC2 and were analyzed for their interacting partners, using standard SDS-PAGE and IB techniques.

mimicking drug targeting of the kinase domain of WNK1, demonstrated that WNK1 catalytic activity was required for the inhibitory phosphorylation of KCC2 at Thr⁹⁰⁶ and Thr¹⁰⁰⁷, and antagonism of WNK1 enhanced KCC2 activity by promoting the dephosphorylation at these sites.

As a ubiquitously expressed kinase, WNK1 can contribute to the control of many other molecules, including KCC3 (26), NKCC1 (38), and potentially other transporters and channels. Here, we performed some experiments in the presence of the NKCC1 inhibitor bumetanide to isolate the contribution of the WNK1-KCC2 pathway to the control of Cl⁻ homeostasis. Future projects will determine the contribution of the WNK1-dependent NKCC1 pathway and its interplay with KCC2-dependent Cl⁻ extrusion in neuronal development and pathological conditions.

Previous studies suggested the existence of at least two distinct mechanisms of KCC2 regulation during development, including growth factor-dependent increases in KCC2 transcription (51, 52) and the posttranslational

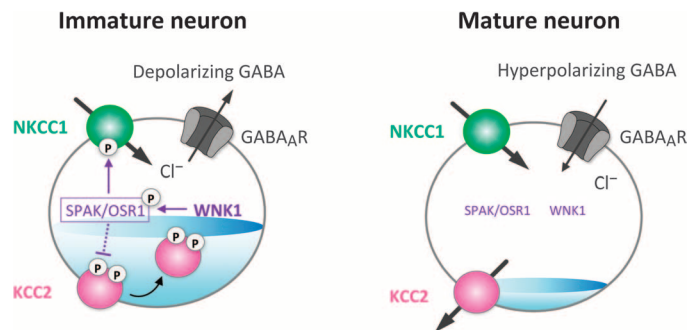


Fig. 8. A model of WNK1-dependent control of neuronal Cl⁻ during development. In immature neurons, the activity of KCC2 is low, such that NKCC1-mediated Cl⁻ loading predominates, and the intraneuronal Cl⁻ concentration [Cl⁻]_i is relatively high. Consequently, GABA_AR activation elicits membrane depolarization. In mature neurons, KCC2-mediated Cl⁻ extrusion predominates, [Cl⁻]_i is low, and GABA_AR activation triggers membrane hyperpolarization. WNK1 contributes to the depolarizing action of GABA in immature neurons by maintaining the inhibitory phosphorylation of KCC2 at Thr⁹⁰⁶ and Thr¹⁰⁰⁷. WNK1 regulates the phosphorylation of KCC2 at Thr¹⁰⁰⁷ through SPAK and at Thr⁹⁰⁶ through a yet unidentified kinase. WNK1-dependent phosphorylation may activate NKCC1 in neurons through a SPAK-dependent mechanism, as occurs in other cell types. We propose that as neurons mature, WNK1-dependent NKCC1 and KCC2 phosphorylation decreases and thereby contributes to the developmental switch in GABA_AR-mediated responses.

regulation of KCC2 activity by (de)phosphorylation (25, 52). In immature neurons, KCC2 is phosphorylated and almost completely inactive despite the presence of KCC2 in neurons of this stage of development (15, 19). Indeed, previous studies showed that phosphorylation at Thr⁹⁰⁶ is reduced 33% by P3 and >90% by P21; in the adult, when the ion transport activity of KCC2 is maximal (14, 19), phosphorylation at Thr⁹⁰⁶ is negligible (16). Despite this inverse correlation between the amount of KCC2 phosphorylation at these sites and transporter activity, little experimental data have linked these two phenomena. Two studies showed that staurosporine, a broad kinase inhibitor, rapidly stimulates KCC2 activity in immature, but not more mature, cultured hippocampal neurons (19) and in immature (E18.5), but not in more mature (P7), cortical slices (24). Here, we identified WNK1 as a specific kinase that contributes to the developmental control of KCC2 activity, revealed a likely mechanism of action for this inhibitory effect of WNK1 (promoting Thr⁹⁰⁶ and Thr¹⁰⁰⁷ phosphorylation of KCC2), and showed that inhibition of an analog-sensitive WNK1 enhanced Cl⁻ extrusion.

What are the factors contributing to the maintenance of a high level of KCC2 inhibitory phosphorylation and low level of its activity? One could be ongoing neuronal activity. Immature neuronal networks in organisms from worms to primates are characterized by the existence of ongoing neuronal activity and synchronous oscillations of intracellular Ca²⁺ that result from the synergistic depolarizing actions of both GABA and glutamate (41). During development, the strength of the depolarizing action of GABA decreases because of progressive increase in KCC2-mediated Cl⁻ extrusion, and ongoing synchronous GABA-driven neuronal activity ceases. In developing neurons, prolonged inhibition of spontaneous network activity triggers a slow reduction in KCC2 activity (53–55). Whether this phenomenon is related to KCC2 phosphorylation at Thr⁹⁰⁶ and Thr¹⁰⁰⁷ remains unknown. A second putative regulatory mechanism might involve taurine, an abundant free amino acid in the brain, that contributes into KCC2 inactivation in immature, but not in mature, neurons (24).

The WNK serine-threonine kinases are master regulators of CCCs (7) and are sensors of $[Cl^-]_i$, extracellular osmolarity, and cell volume. WNKs transduce signals about changes in these parameters to the CCCs to regulate transporter activity. The *PRKWINK1* gene encodes multiple alternatively spliced WNK1 isoforms. One isoform is mutated in Mendelian disease featuring impaired Cl^- transport in the distal nephron causing hypertension (30). Multiple full-length WNK1 isoforms, including the *HSN2* splice variant that is mutated in congenital pain insensitivity, are prominently expressed in embryonic and early postnatal brain and particularly in the CA1, CA2, and CA3 areas of the hippocampus (34, 36) and in the cortex (24), suggesting a role in brain development. *PRKWINK1* expression, in contrast to *PRKWINK2* and *PRKWINK3*, declines in adulthood in these brain regions (34, 36).

WNK-mediated regulation of the CCCs is triggered by an interaction between RFXV/I motifs within the WNKs and CCCs and a conserved C-terminal docking domain in the kinases SPAK and OSR1. WNKs directly phosphorylate SPAK and OSR1, which in turn phosphorylate KCC2 at Thr¹⁰⁰⁷ but not Thr⁹⁰⁶ (26). The kinase regulating KCC2 Thr⁹⁰⁶ phosphorylation remains unknown. However, WNK1 knockdown in HEK293 cells decreases KCC3 phosphorylation at Thr⁹⁹¹, a site homologous to Thr⁹⁰⁶ in KCC2 (16). Given the similar effects of WNK1 shRNA, WNK1-DN, and chemical inhibition of WNK on KCC2 activity, we concluded that WNK1 is required for and regulates the phosphorylation of KCC2 at both Thr⁹⁰⁶ and Thr¹⁰⁰⁷ in a kinase-dependent manner. However, our results indicated that WNK1 is likely not the direct phosphorylating kinase at either Thr⁹⁰⁶ or Thr¹⁰⁰⁷. Further experiments are required to identify the kinase that phosphorylates KCC2 at Thr⁹⁰⁶, as well as the stimuli that reduce WNK1-mediated KCC2 inhibition during development.

Our chemical genetic work has established a new tool for studying WNK signaling, allowing for the specific and dynamic modulation of WNK1 kinase activity in a cellular context. This technique exploits a functionally silent mutation in the catalytic active site to sensitize a target kinase to small-molecule inhibition that does not inhibit wild-type kinases (56). This is of particular relevance for the WNK family, which contains multiple family members and splice variants, and for which no current pharmacological inhibitors exist, thus allowing the differentiation between WNK1 and other family members. Chemical genetic experiments with WNK1 might also enable the specific study of WNK1 function in vivo, for example, in knock-in mice created with the WNK1-AS mutation, which would overcome the embryonic lethality of WNK1 knockout in (57).

Finally, our results in neurons suggested that inhibition of WNK signaling in the CNS might be a means of enhancing neuronal Cl^- extrusion to restore GABAergic inhibition by stimulating KCC2. This might be of value for neuropsychiatric conditions in which KCC2 activity is suppressed and GABAergic disinhibition fosters the hyperexcitability of neurons and circuits. This strategy may be particularly relevant in the immature brain in which KCC2 phosphorylation is highest, and therefore of interest in studying neurodevelopmental disorders, like autism (58) or neonatal seizures (59), which reveal pathologic excitatory GABA responses due to increased neuronal Cl^- concentrations at time points when KCC2 is likely present but functionally inhibited. Moreover, it is tempting to speculate that inhibitory KCC2 Thr⁹⁰⁶ and Thr¹⁰⁰⁷ phosphorylation might also be pathologically increased in mature neurons, accounting for the documented decrease in KCC2-mediated Cl^- extrusion capacity and GABAergic disinhibition in diseases, such as temporal lobe epilepsy (60) and neuropathic pain (61). Mutations in KCC2 associated with human disease, severe idiopathic generalized epilepsy in a large French Canadian patient cohort (43) and febrile seizures in an Australian family (62), are clustered in the C-terminal region and reside in residues close to the Thr⁹⁰⁶ and

Thr¹⁰⁰⁷ motifs, which would likely alter KCC2 activity. These subjects will be rich topics of future investigations with potential clinical relevance.

MATERIALS AND METHODS

Constructs and materials

Human *WNK1* in the *pCS2* vector with a cytomegalovirus promoter, containing exons 1 to 28, including the *HSN2* exon but excluding exons 11 and 12, and engineered to express c6 N-terminal Myc tags, was previously described (63). This construct was used for biochemistry. For electrophysiology, the full-length insert minus the Myc tag was cloned into a vector containing an N-terminal mCherry tag. Other constructs included HA-tagged KCC2 (gift from C. Rivera), HA-tagged OSR1 (38), eGFP and mCherry (Clontech), rat mCherry-KCC2 (40), rat KCC2-pHluorin [pHluorin was introduced in the second extracellular loop of KCC2, (43)], and *Cl-Sensor* in *gw1* vector (64). All mutations were generated using the QuikChange (Stratagene) site-directed method and were verified by DNA sequencing.

shRNA KCC2 in *mU6-pro* vector was described previously (39) and targeted the following sequence in rat KCC2 mRNA: 5'-GACATTGGTAA-TGGAACAACG-3' (NP_599190). A control construct with a scrambled sequence (GATGAACCTGATGACGTTTC) lacked homology to any known mammalian mRNAs. shRNA WNK1 (OriGene Technologies Inc., in pRFP-C-RS retroviral vector) targeted the 5'-CATTGAGATGTTGCTTCTGGTATGAGTGA-3' sequence of rat WNK1 mRNA (NM_001002823) and is predicted to knock down known isoforms of *WNK1* in the brain, including *HSN2*.

For the characterization of WNK1 shRNA, rat PC12 cells were transfected with control firefly (FF) luciferase (*luc*) shRNA (65) or rat WNK1 shRNA in a puromycin-resistant vector (pRFP-C-RS, OriGene) with FuGENE 6 (Roche Applied Science) at a 3:1 ratio (DNA/transfection reagent) according to the manufacturer's directions. Transfected cells were incubated for 48 hours before the addition of puromycin (8 μ g/ml). After selection, lysates were harvested, subjected to SDS-PAGE, and assessed by Western blotting.

PC12 (CRL-1721) and N2a (CCL-131) cell lines were obtained from the American Type Culture Collection and processed according to the manufacturer's guidelines. All transfections of these cell lines were performed using Lipofectamine 2000 (Life Technologies). For the transfection of cells growing in 35-mm culture dishes, a mixture of 300 μ l of Opti-MEM (Life Technologies), 7 μ l of Lipofectamine 2000, and 1.5 μ g of pcDNAs encoding the desired constructs was prepared. The mixture was kept for 15 min at room temperature to form the Lipofectamine-pcDNA complex and was distributed dropwise above the cells.

Animals

Animal care and handling was performed in accordance with the guidelines of the European Union Council and the INSERM regulations on the use of laboratory animals.

Primary cultures and transfection of rat hippocampal neurons

Hippocampi and cortices from 18-day-old rat embryos were dissected and dissociated using trypsin (0.05%) and plated at a density of 70,000 cells cm^{-2} in minimal essential medium (MEM) supplemented with 10% Nu-Serum (BD Biosciences), 0.45% glucose, 1 mM sodium pyruvate, 2 mM glutamine, and penicillin-streptomycin (10 IU ml^{-1}) as previously described (66). On days 7, 10, and 13 of culture incubation, half of the medium was changed to MEM with 2% B27 supplement (Invitrogen).

For immunocytochemistry, electrophysiology, and noninvasive Cl-Sensor analysis, neuronal cultures were plated on coverslips placed in 35-mm culture dishes. Twenty-four hours before plating, dishes with coverslips were coated with polyethylenimine (5 µg/ml). For physiology and immunocytochemistry experiments, neurons were plated in 35-mm culture dishes containing 14-mm coverslips. For Western blot experiments, neurons were plated in 60-mm dishes (four dishes per culture and div).

Transfections of neuronal cultures were performed at 4 div (for recordings on 6 to 7 div) and 10 div (for recordings on 13 to 15 div) as described previously (66). For transfection of cultures growing in 35-mm dishes, 300 µl of Opti-MEM was mixed with 7 µl of Lipofectamine 2000 (Invitrogen), 1 µl of Magnetofection CombiMag (OZ Biosciences), and 1 to 1.5 µg of different pcDNAs premixed in desired proportions. The mixture was incubated for 20 min at room temperature and thereafter distributed dropwise above the neuronal culture. Culture dishes were placed on a magnetic plate (OZ Biosciences) and incubated for 30 to 35 min at 37°C. Transfection was terminated by the substitution of 90% of the incubation solution with fresh culture medium.

Most of the experiments were based on cotransfection into the same cell of two or three different pcDNAs encoding a fluorescent marker of transfection (eGFP or Cl-Sensor), shRNAs, WNK1 constructs, and with or without mutants of KCC2. Before electrophysiology or imaging experiments, we specifically studied the efficacy of neuronal cotransfection with mixtures of pcDNAs in different proportions as described in (39). A mixture containing 0.15 + 0.6 + 0.6 µg for cotransfection of three constructs

(marker + shRNA + KCC2 or marker + WNK1 + KCC2) ensured the expression of both constructs of interest into the eGFP-positive or Cl-Sensor-positive neurons or N2a cells. For transfection of two constructs, we routinely used mixtures of 0.2 µg of marker + 1.0 µg of the construct of interest.

Antibodies

Primary antibodies used for immunocytochemistry included polyclonal rabbit anti-GFP (Molecular Probes, Life Technologies) and monoclonal mouse anti-GFP (Novus Biologicals, Interchim). The secondary antibodies included anti-mouse Alexa 488 (dilution, 1:1000; FluoProbes, Interchim); anti-rabbit Cy3 (dilution, 1:1000; Jackson ImmunoResearch Laboratories Inc.).

Antibodies used for Western blots included antibodies raised in sheep and affinity-purified on the appropriate antigen by the Division of Signal Transduction Therapy at the University of Dundee; other antibodies were purchased (Table 1). Secondary antibodies coupled to horseradish peroxidase (HRP) used for immunoblotting were obtained from Pierce. Immunoglobulin G used in control immunoprecipitation experiments was affinity-purified from preimmune serum using protein G–Sepharose.

Buffers for Western blots

Buffer A contained 50 mM tris-HCl (pH 7.5) and 0.1 mM EGTA. Lysis buffer contained 50 mM tris-HCl (pH 7.5), 1 mM EGTA, 1 mM EDTA, 50 mM sodium fluoride, 5 mM sodium pyrophosphate, 1 mM sodium orthovanadate, 1% (w/v) Triton X-100, 0.27 M sucrose, 0.1% (v/v) 2-mercaptoethanol, and protease inhibitors (complete protease inhibitor cocktail tablets, Roche;

Table 1. List of antibodies used in Western blotting and immunoprecipitation. Phosphorylated residues in the amino acid sequences are in parentheses.

| Antibody | Antigen | Rat corresponding sequence | Species | Source |
|---|---|---|---------|-----------------------|
| KCC2A phospho-Thr ⁹⁰⁶ | SAYTYER(T)LMMEQRSRR (residues 975–989 of human KCC3A) corresponding to SAYTYEK(T)LVMEQRSQI (residues 899–915 of human KCC2A) | SAYTYEK(T)LVMEQRSQI (residues 899–915 of rat KCC2) | Sheep | Dundee (S959C) |
| KCC2A phospho-Thr ¹⁰⁰⁶ | CYQEKVHM(T)WTKDKYM (residues 1032–1046 of human KCC3A) corresponding to TDPEKVHL(T)WTKDKSVA (residues 998–1014 of human KCC2A) | TDPEKVHL(T)WTKDKSAA (residues 998–1014 of rat KCC2) | Sheep | Dundee (S961C) |
| NKCC1 total | Residues 1–288 of human NKCC1 (DU 34492) | Residues 1–279 of rat NKCC1 | Sheep | Dundee (S022D) |
| NKCC1 phospho-Thr ²⁰³ / Thr ²⁰⁷ /Thr ²¹² | HYYYD(T)HTN(T)YYLR(T)FGHNT (residues 198–217 of human NKCC1 phosphorylated at Thr ²⁰³ , Thr ²⁰⁷ , and Thr ²¹²) | QYYVD(T)HTN(T)YYLR(T)FGHNT (residues 189–208 of rat NKCC1 phosphorylated at Thr ¹⁹⁴ , Thr ¹⁹⁸ , and Thr ²⁰³) | Sheep | Dundee (S763B) |
| WNK1 total | Residues 2360–2382 of human WNK1 | Residues 2613–2634 of rat WNK1 | Sheep | Dundee (S469D) |
| WNK1 phospho-Ser ³⁸² | ASFAK(S)VIGTP (residues 377–387 of human WNK1 phosphorylated at Ser ³⁸²) | ASFAK(S)VIGTP (residues 377–387 of rat WNK1 phosphorylated at Ser ³⁸²) | Sheep | Dundee (S099B) |
| SPAK total | Full-length glutathione S-transferase-tagged human SPAK protein | | Sheep | Dundee (S551D) |
| OSR1 total | RSAHLPQPAGQMPTQPAQVSLR (residues 389–408 of mouse OSR1) | RSAHLPQPAGQMPTQPASVSLR (residues 389–408 of rat OSR1) | Sheep | Dundee (S850C) |
| SPAK/OSR1 (S-motif) phospho-Ser ³⁷³ / Ser ³²⁵ | RRVPGS(S)GHLHKT (residues 367–379 of human SPAK), which is highly similar to residues 319–331 of human OSR1 in which the sequence is RRVPGS(S)GRLHKT | RRVPGS(S)GHLHKT (residues 376–388 of rat SPAK) | Sheep | Dundee (S670B) |
| ERK1 total | Full-length human ERK1 protein | | Sheep | Dundee (S221B) |
| Pan-KCC2 total | Residues 932–1043 of human KCC2 | Residues 932–1043 of rat KCC2 | Mouse | NeuroMab (73-013) |
| β-Tubulin III (neuronal) | Residues 436–450 of human neuronal specific β-tubulin III; has one amino acid difference in rat and mouse β-tubulin III. | Residues 436–450 of rat neuronal specific β-tubulin III | Mouse | Sigma-Aldrich (T8578) |

Downloaded from <http://stke.sciencemag.org/> on June 28, 2019

1 tablet per 50 ml). Tween–tris–buffered saline (TTBS) contained tris-HCl (pH 7.5), 0.15 M NaCl, and 0.2% (v/v) Tween 20. SDS sample buffer consisted of 1× NuPAGE LDS sample buffer (Invitrogen) containing 1% (v/v) 2-mercaptoethanol. Protein concentrations were determined after centrifugation of the lysate at 16,000g at 4°C for 20 min using the Bradford method with bovine serum albumin as the standard.

Immunoprecipitation with phosphorylation site-specific antibodies

KCCs phosphorylated at the KCC2 Thr⁹⁰⁶ and Thr¹⁰⁰⁷ equivalent residue were immunoprecipitated from clarified hippocampal and cortical culture lysates (centrifuged at 16,000g at 4°C for 20 min) using phosphorylation site-specific antibody coupled to protein G–Sepharose as described (26). The phosphorylation site-specific antibody was coupled with protein G–Sepharose at a ratio of 1 mg of antibody per 1 ml of beads in the presence of lysate (20 µg/ml) to which the corresponding nonphosphorylated peptide had been added. Two milligrams of clarified cell lysate was incubated with 15 µg of antibody conjugated to 15 µl of protein G–Sepharose for 2 hours at 4°C with gentle agitation. Beads were washed three times with 1 ml of lysis buffer containing 0.15 M NaCl and twice with 1 ml of buffer A. Bound proteins were eluted with 1× LDS sample buffer.

Immunoblotting

Cell lysates (15 µg) in SDS sample buffer were subjected to electrophoresis on polyacrylamide gels and transferred onto nitrocellulose membranes. The membranes were incubated for 30 min with TTBS containing 5% (w/v) skim milk. The membranes were then immunoblotted in 5% (w/v) skim milk in TTBS with the indicated primary antibodies overnight at 4°C. Antibodies prepared in sheep were used at a concentration of 1 to 2 µg/ml. The incubation with phosphorylation site-specific sheep antibodies was performed with the addition of the nonphosphorylated peptide antigen (10 µg/ml) (Table 1) used to raise the antibody. The blots were then washed six times with TTBS and incubated for 1 hour at room temperature with secondary HRP-conjugated antibodies diluted 5000-fold in 5% (w/v) skim milk in TTBS. After repeating the washing steps, the signal was detected with the enhanced chemiluminescence reagent. Immunoblots were developed using a film automatic processor (SRX-101; Konica Minolta Medical), and films were scanned with a 600-dpi resolution on a scanner (PowerLook 1000, UMAX). Figures were generated using Photoshop and Illustrator (Adobe). The relative intensities of immunoblot bands were determined by densitometry with ImageJ software.

Electrophysiology recordings

The gramicidin-perforated whole-cell patch-clamp recordings from transfected neurons (eGFP-positive) were performed according to protocols described previously (39, 67). The external solution contained 140 mM NaCl, 2.5 mM KCl, 20 mM Hepes, 20 mM D-glucose, 2.0 mM CaCl₂, 2.0 mM MgCl₂, 0.001 mM tetrodotoxin, and 0.0003 mM strychnine (pH 7.4). Coverslips with transfected neuronal cells were placed onto an inverted microscope and perfused with a fast perfusion system placed in front of the recording neuron to ensure removal of trace amounts of gramicidin that could diffuse from the patch pipette. Patch pipettes (5 megohms) were filled with a solution containing 150 mM KCl, 10 mM Hepes, and 20 mM gramicidin A (pH 7.2). The gigaseals were formed by rapid 5- to 10-s approaching of the patch pipette to neuronal surface without applying positive pressure (to diminish leak of gramicidin). After sealing, series resistance (R_s), membrane resistance (R_m), and neuron capacitance (C) were monitored routinely at a V_h of -80 mV with 5-mV hyperpolarizing pulses, typically taking 10 to 15 min for the series resistance to stabilize at

15 to 60 megohms. Membrane potential values were corrected offline for junction potential between the pipette and bath solutions (-4.0 mV) and series resistance as described (68, 69).

Isoguvacine (30 µM) was focally applied to the neuron soma and proximal dendrites through a micropipette connected to a Picospritzer (General Valve Corporation). The pipette position, pulse duration (50 to 150 ms), and pressure (10,000 to 30,000 Pa) were adjusted for each neuron by applying test pulses at V_h of -80 and -60 mV with the final aim of producing currents with the slope of current-voltage relationship ($I-V$) below 4.0 pA mV⁻¹. This procedure minimized changes in $[Cl^-]_i$ during $I-V$ recording. Depending on the direction of the above test currents, four isoguvacine responses were then recorded at voltages -120 , -100 , -80 , and -60 mV [for neurons showing outwardly directed (positive) responses at both -80 and -60 mV]; -100 , -80 , -60 , and -40 mV [for neurons showing outward responses at -80 and inward (negative) responses at -60 mV]; or -80 , -60 , -40 , and -20 mV (for inwardly directed isoguvacine-induced responses at -60 mV) as shown in Fig. 1A.

All experiments were performed at 23° to 24°C. Recordings were made using an Axopatch 200A amplifier and pCLAMP acquisition software (Axon Instruments). Data were low pass-filtered at 2 kHz and acquired at 10 kHz.

In utero electroporation

In utero injections and electroporations were performed as previously described (70) in embryos from timed pregnant rats (embryonic day 15) that were anesthetized with ketamine (100 mg/kg; IMALGENE 1000, Merial)/xylazine (10 mg/kg; Rompun 2%, Bayer Healthcare). Wistar rats (Janvier) were raised and mated at INMED (Institut de Neurobiologie de la Méditerranée) Post-Genomic Platform animal facility in agreement with the European Union and French legislations. The uterine horns were exposed, and a lateral ventricle of each embryo was injected using pulled glass capillaries and a microinjector (PV820 Pneumatic PicoPump, World Precision Instruments) with Fast Green (2 mg/ml; Sigma) combined with the constructs encoding Cl-Sensor plus scrambled shRNA or WNK1 shRNA (ratio 1:3). Plasmids were further electroporated by discharging a 4000-µF capacitor charged to 40 V with a BTX ECM 830 electroporator (BTX Harvard Apparatus). The voltage was discharged in five electrical pulses at 950-ms intervals through tweezer-type electrodes placed on the head of the embryo across the uterine wall. We performed in utero electroporation in embryonic rats at E15, corresponding to an active period of both radial and tangential migration of newborn neurons in the cortex.

Cl-Sensor fluorescence recordings from brain slices

Experiments were performed on acute transverse cortical slices (350 µm) that were cut using a vibratome (VT1000E, Leica) into ice-cold (2° to 4°C) ACSF composed of 126 mM NaCl, 3.5 mM KCl, 2 mM CaCl₂, 1.3 mM MgCl₂, 1.2 mM NaH₂PO₄, 25 mM NaHCO₃, and 11 mM glucose (pH 7.4) when equilibrated with 95% O₂ and 5% CO₂. Slices were maintained in oxygenated (95% O₂ and 5% CO₂, pH 7.3) ACSF at room temperature for at least 1 hour before use. Individual slices were transferred to a specially designed recording chamber where they were fully submerged and perfused with oxygenated ACSF [complemented with 1 µM tetrodotoxin, 1 µM strychnine, and 10 µM NBQX (6-nitro-7-sulfamoylbenzo[*q*]quinoxaline-2,3-dione) to prevent spontaneous neuronal activity and noncontrolled $[Cl^-]_i$ changes] at 30° to 32°C at a rate of 2 to 3 ml/min. The acquisition of fluorescence images was performed using a customized imaging setup and consecutive cell excitation at 430 and 500 nm as described previously (40). The frequency of acquisition was 0.05 Hz. The duration of excitation was selected to avoid use-dependent bleaching of the signal and was identical for all experiments (40). The applications of the ACSF solution

containing isoguvacine (30 μ M) or KCl (25 mM) + isoguvacine (30 μ M) were performed with a perfusion system. The recovery of fluorescence after Cl^- overload produced by KCl + isoguvacine was recorded in ACSF containing 10 μ M bicuculline in addition to the abovementioned blockers to avoid Cl^- efflux through GABA_AR .

Immunocytochemistry and quantitative immunofluorescence analysis of primary neuronal cultures

For immunocytochemistry on living neurons, rabbit antibodies against GFP were diluted in culture medium and applied to neurons for 2 hours at 37°C, 5% CO_2 . Neurons were then washed for 10 min at room temperature in Hepes-buffered saline solution containing 150 mM NaCl, 2.5 mM KCl, 2.0 mM MgCl_2 , 2.0 mM CaCl_2 , 20 mM Hepes, and 10 mM D-glucose (pH 7.4), labeled with anti-rabbit Cy3 antibody (dissolved in the Hepes-buffered saline) for 20 min at 13°C and fixed in Antigenfix (Diapath). To reveal intracellular proteins, cells were subsequently permeabilized with 0.3% Triton X-100, blocked by 5% goat serum, labeled overnight (4°C) with mouse antibody against GFP and for 1 hour at room temperature with anti-mouse Alexa 488 antibody. Cell nuclei were stained by 5-min incubation with Hoechst 33258 (1 μ g/ml; Sigma-Aldrich).

For quantitative analysis, images were acquired with an Olympus FluoView-500 confocal microscope [oil immersion objectives, 40 \times [numerical aperture (NA) 1.0] or 60 \times (NA 1.4); zoom 1 to 5]. We randomly selected and focused on a transfected neuron by visualizing eGFP or pHluorin fluorescence and then acquired images of membrane clusters. The cluster properties of each cell were analyzed with MetaMorph software (Roper Scientific SAS). First, we created a binary mask of eGFP or pHluorin-fluorescent cells and then analyzed KCC2 membrane fluorescence in regions overlapping with the binary mask. Analysis parameters were the same for all experimental conditions. All experiments were performed in a blinded manner. After analysis, data were normalized to the mean value of cells transfected with KCC2-pH_{ext}.

Generation of an analog-sensitive WNK1 kinase

To make WNK1-AS, which can utilize bulky ATP analogs instead of ATP and be inhibited by kinase inhibitors such as 1-NA-PP1 (44), we mutated the WNK1-CA ATP binding pocket gatekeeper threonine to alanine (T301A) on the basis of homology searches with other kinases in which this method has been successfully used (46). Many protein kinases tolerate replacement of the gatekeeper mutation to alanine, which enlarges the catalytic pocket enough to accommodate bulky purine analogs; however, 20% of all kinases exhibit decreased activity when this residue is mutated unless a suppressor mutation in the amino-terminal lobe of the ATP binding pocket is also present (71). We therefore engineered the I357L and G367A mutations in the WNK1-CA T301A kinase domain. This combination of mutations yielded an analog-sensitive WNK1 capable of phosphotransfer of N^6 -substituted ATP- γ -S (N^6 -benzyl-ATP- γ -S) to substrates and inhibition in the micromolar range by 1-NA-PP1.

Thiophosphorylation of kinase substrates in cellular lysates

The following method was used to determine if OSR1 or KCC2 was a substrate of WNK1-AS in a complex protein mixture, as described in detail (44). Briefly, Myc-tagged WNK1-AS, WNK1-DN, or WNK1-CA was transiently coexpressed with HA-OSR1 or HA-KCC2 in N2a cells cultured in 10-cm dishes. After 48 hours, cells were treated with 1-NA-PP1 (1 or 10 μ M) or vehicle control (dimethyl sulfoxide) for 2 hours before the medium was removed. Cells were then rinsed once with 5 ml of cold phosphate-buffered saline (pH 7.4), harvested with a scraper, and

lysed on ice in 500 μ l of 1 \times standard radioimmunoprecipitation assay (RIPA) buffer + 1 \times protease inhibitor + 1 \times phosphatase inhibitor. Cells were then centrifuged at 10,000g for 10 min at 4°C to remove cell debris. Supernatant was saved, and to the supernatant was added 100 μ M N^6 -benzyl-ATP- γ -S, 100 μ M ATP, and 3 mM guanosine triphosphate (GTP) to initiate the substrate labeling reaction. Samples were incubated for 20 min at room temperature. The reaction was quenched with 500 μ l of 1 \times RIPA buffer + 40 mM EDTA (final [EDTA] = 20 mM) + 5 mM *p*-nitrobenzyl mesylate (PNBM) (final [PNBM] = 2.5 mM), and then alkylated with PNBM for 1 hour at room temperature on a rotator. Each sample then received 40 μ l of a 50% slurry of appropriate antibody-tagged magnetic beads (Bethyl Laboratories) and was incubated for 3 to 4 hours at 4°C on a rotator. Before use, beads were washed once with 1 ml of 1 \times RIPA buffer and then resuspended in the original slurry volume. A magnet was used to collect the beads, which were washed five times with 1 ml of 1 \times RIPA + protease inhibitor + phosphatase inhibitor and then resuspended in 20 μ l of 1 \times RIPA + protease inhibitor + phosphatase inhibitor + 1 \times Laemmli sample buffer. Samples were heated at 95°C for 2.5 min and then loaded onto an SDS-PAGE gel. Western blotting was performed with antibodies recognizing HA or Myc or a rabbit monoclonal antibody recognizing the thiophosphate ester (Epitomics). Assays with phosphorylation site-specific antibodies recognizing KCC2 were performed essentially as described in (26), using N2a cells cotransfected with the Myc-tagged WNK1 plasmids and HA-tagged KCC2.

Statistical analysis

For the electrophysiology recordings, each condition (such as neurons with shRNA WNK1) was studied during at least four experiments (transfections), with one to three neurons per experiment. On the same experimental day, at least two other conditions were analyzed (for example, shRNA WNK1 + WNK-CA and scrambled shRNA). The population data were expressed as mean \pm SEM, where *n* was the number of recorded neurons. For analysis of fluorescence, the mean value recorded from multiple neurons located in the optical field was taken as a single measurement (experiment). The mean values \pm SEM were results of analysis with the indicated number (*n*) of experiments. The one-way ANOVA or nonparametric Mann-Whitney test was performed to examine the statistical significance of the differences between groups of data, unless otherwise indicated.

SUPPLEMENTARY MATERIALS

www.sciencesignaling.org/cgi/content/full/8/383/ra65/DC1

Fig. S1. Characterization of a specific WNK1 shRNA.

Fig. S2. Quantification of the abundance of phosphorylated KCC2 species by Western blot.

Fig. S3. Characterization of a WNK1-AS construct.

REFERENCES AND NOTES

1. F. Lang, Mechanisms and significance of cell volume regulation. *J. Am. Coll. Nutr.* **26**, 613S–623S (2007).
2. K. B. Gagnon, E. Delpire, Physiology of SLC12 transporters: Lessons from inherited human genetic mutations and genetically engineered mouse knockouts. *Am. J. Physiol. Cell Physiol.* **304**, C693–C714 (2013).
3. P. Blaesse, M. S. Airaksinen, C. Rivera, K. Kaila, Cation-chloride cotransporters and neuronal function. *Neuron* **61**, 820–838 (2009).
4. K. T. Kahle, J. Rinehart, A. Ring, I. Gimenez, G. Gamba, S. C. Hebert, R. P. Lifton, WNK protein kinases modulate cellular Cl^- flux by altering the phosphorylation state of the Na-K-Cl and K-Cl cotransporters. *Physiology* **21**, 326–335 (2006).
5. R. Planells-Cases, T. J. Jentsch, Chloride channelopathies. *Biochim. Biophys. Acta* **1792**, 173–189 (2009).
6. J. P. Arroyo, K. T. Kahle, G. Gamba, The SLC12 family of electroneutral cation-coupled chloride cotransporters. *Mol. Aspects Med.* **34**, 288–298 (2013).
7. D. R. Alessi, J. Zhang, A. Khanna, T. Hochdörfer, Y. Shang, K. T. Kahle, The WNK-SPAK/OSR1 pathway: Master regulator of cation-chloride cotransporters. *Sci. Signal.* **7**, re3 (2014).

8. K. T. Kahle, A. M. Ring, R. P. Lifton, Molecular physiology of the WNK kinases. *Annu. Rev. Physiol.* **70**, 329–355 (2008).
9. E. J. Hoon, D. H. Ellison, WNK kinases and the kidney. *Exp. Cell Res.* **318**, 1020–1026 (2012).
10. S. L. Deaton, S. Sengupta, M. H. Cobb, WNK kinases and blood pressure control. *Curr. Hypertens. Rep.* **11**, 421–426 (2009).
11. S. Uchida, Pathophysiological roles of WNK kinases in the kidney. *Pflugers Arch.* **460**, 695–702 (2010).
12. M. Farrant, K. Kaila, The cellular, molecular and ionic basis of GABA_A receptor signalling. *Prog. Brain Res.* **160**, 59–87 (2007).
13. Y. Ben-Ari, I. Khalilov, K. T. Kahle, E. Cherubini, The GABA excitatory/inhibitory shift in brain maturation and neurological disorders. *Neuroscientist* **18**, 467–486 (2012).
14. C. Rivera, J. Voipio, J. A. Payne, E. Ruusuvuori, H. Lahtinen, K. Lamsa, U. Pirvola, M. Saarna, K. Kaila, The K⁺/Cl⁻ co-transporter KCC2 renders GABA hyperpolarizing during neuronal maturation. *Nature* **397**, 251–255 (1999).
15. V. Stein, I. Hermans-Borgmeyer, T. J. Jentsch, C. A. Hübner, Expression of the KCl cotransporter KCC2 parallels neuronal maturation and the emergence of low intracellular chloride. *J. Comp. Neurol.* **468**, 57–64 (2004).
16. J. Rinehart, Y. D. Maksimova, J. E. Tanis, K. L. Stone, C. A. Hodson, J. Zhang, M. Risinger, W. Pan, D. Wu, C. M. Colangelo, B. Forbush, C. H. Joiner, E. E. Gulcicek, P. G. Gallagher, R. P. Lifton, Sites of regulated phosphorylation that control K-Cl cotransporter activity. *Cell* **138**, 525–536 (2009).
17. P. Blaesse, I. Guillemin, J. Schindler, M. Schweizer, E. Delpire, L. Khiroug, E. Friauf, H. G. Nothwang, Oligomerization of KCC2 correlates with development of inhibitory neurotransmission. *J. Neurosci.* **26**, 10407–10419 (2006).
18. L. Zhu, N. Polley, G. C. Mathews, E. Delpire, NKCC1 and KCC2 prevent hyperexcitability in the mouse hippocampus. *Epilepsy Res.* **79**, 201–212 (2008).
19. S. Khirug, K. Huttu, A. Ludwig, S. Smirnov, J. Voipio, C. Rivera, K. Kaila, L. Khiroug, Distinct properties of functional KCC2 expression in immature mouse hippocampal neurons in culture and in acute slices. *Eur. J. Neurosci.* **21**, 899–904 (2005).
20. I. Khalilov, G. Chazal, I. Chudotvorova, C. Pellegrino, S. Corby, N. Ferrand, O. Gubkina, R. Nardou, R. Tyzio, S. Yamamoto, T. J. Jentsch, C. A. Hübner, J.-L. Gaiarsa, Y. Ben-Ari, I. Medina, Enhanced synaptic activity and epileptiform events in the embryonic KCC2 deficient hippocampus. *Front. Cell. Neurosci.* **5**, 23 (2011).
21. Y. Ben-Ari, E. Cherubini, R. Corradetti, J. L. Gaiarsa, Giant synaptic potentials in immature rat CA3 hippocampal neurones. *J. Physiol.* **416**, 303–325 (1989).
22. R. Khazipov, I. Khalilov, R. Tyzio, E. Morozova, Y. Ben-Ari, G. L. Holmes, Developmental changes in GABAergic actions and seizure susceptibility in the rat hippocampus. *Eur. J. Neurosci.* **19**, 590–600 (2004).
23. H. H. Lee, T. Z. Deeb, J. A. Walker, P. A. Davies, S. J. Moss, NMDA receptor activity downregulates KCC2 resulting in depolarizing GABA_A receptor-mediated currents. *Nat. Neurosci.* **14**, 736–743 (2011).
24. K. Inoue, T. Furukawa, T. Kumada, J. Yamada, T. Wang, R. Inoue, A. Fukuda, Taurine inhibits K⁺-Cl⁻ cotransporter KCC2 to regulate embryonic Cl⁻ homeostasis via with-nolysine (WNK) protein kinase signaling pathway. *J. Biol. Chem.* **287**, 20839–20850 (2012).
25. K. T. Kahle, T. Z. Deeb, M. Puskarjov, L. Silayeva, B. Liang, K. Kaila, S. J. Moss, Modulation of neuronal activity by phosphorylation of the K–Cl cotransporter KCC2. *Trends Neurosci.* **36**, 726–737 (2013).
26. P. de Los Heros, D. R. Alessi, R. Gourlay, D. G. Campbell, M. Deak, T. J. Macartney, K. T. Kahle, J. Zhang, The WNK-regulated SPAK/OSR1 kinases directly phosphorylate and inhibit the K⁺-Cl⁻ co-transporters. *Biochem. J.* **458**, 559–573 (2014).
27. A. T. Plala, T. M. Moon, R. Akella, H. He, M. H. Cobb, E. J. Goldsmith, Chloride sensing by WNK1 involves inhibition of autophosphorylation. *Sci. Signal.* **7**, ra41 (2014).
28. K. B. Gagnon, E. Delpire, Molecular physiology of SPAK and OSR1: Two Ste20-related protein kinases regulating ion transport. *Physiol. Rev.* **92**, 1577–1617 (2012).
29. L. M. Boyden, M. Choi, K. A. Choate, C. J. Nelson-Williams, A. Farhi, H. R. Toka, I. R. Tikhonova, R. Bjornson, S. M. Mane, G. Colussi, M. Lebel, R. D. Gordon, B. A. Semmekrot, A. Poujol, M. J. Välimäki, M. E. De Ferrari, S. A. Sanjad, M. Gutkin, F. E. Karet, J. R. Tucci, J. R. Stockigt, K. M. Keppler-Noreuil, C. C. Porter, S. K. Anand, M. L. Whiteford, I. D. Davis, S. B. Dewar, A. Bettinelli, J. J. Fadrowski, C. W. Belsha, T. E. Hunley, R. D. Nelson, H. Trachtman, T. R. Cole, M. Pinsk, D. Bockenbauer, M. Shenoy, P. Vaidyanathan, J. W. Foreman, M. Rasoulpour, F. Thameem, H. Z. Al-Shahrouri, J. Radhakrishnan, A. G. Gharavi, B. Gollav, R. P. Lifton, Mutations in kelch-like 3 and cullin 3 cause hypertension and electrolyte abnormalities. *Nature* **482**, 98–102 (2012).
30. F. H. Wilson, S. Disse-Nicodème, K. A. Choate, K. Ishikawa, C. Nelson-Williams, I. Desitter, M. Gunel, D. V. Milford, G. W. Lipkin, J. M. Achard, M. P. Feely, B. Dussol, Y. Berland, R. J. Unwin, H. Mayan, D. B. Simon, Z. Farfel, X. Jeunemaitre, R. P. Lifton, Human hypertension caused by mutations in WNK kinases. *Science* **293**, 1107–1112 (2001).
31. D. B. Simon, R. P. Lifton, Ion transporter mutations in Gitelman's and Bartter's syndromes. *Curr. Opin. Nephrol. Hypertens.* **7**, 43–47 (1998).
32. S. Holden, J. Cox, F. L. Raymond, Cloning, genomic organization, alternative splicing and expression analysis of the human gene *WNK3* (*PRKWINK3*). *Gene* **335**, 109–119 (2004).
33. K. T. Kahle, J. Rinehart, P. de Los Heros, A. Louvi, P. Meade, N. Vazquez, S. C. Hebert, G. Gamba, I. Gimenez, R. P. Lifton, WNK3 modulates transport of Cl⁻ in and out of cells: Implications for control of cell volume and neuronal excitability. *Proc. Natl. Acad. Sci. U.S.A.* **102**, 16783–16788 (2005).
34. J. Rinehart, N. Vazquez, K. T. Kahle, C. A. Hodson, A. M. Ring, E. E. Gulcicek, A. Louvi, N. A. Bobadilla, G. Gamba, R. P. Lifton, WNK2 kinase is a novel regulator of essential neuronal cation-chloride cotransporters. *J. Biol. Chem.* **286**, 30171–30180 (2011).
35. M. Shekarabi, N. Girard, J.-B. Rivière, P. Dion, M. Houle, A. Toulouse, R. G. Lafrenière, F. Vercauteren, P. Hince, J. Laganière, D. Rochefort, L. Faivre, M. Samuels, G. A. Rouleau, Mutations in the nervous system-specific *HSN2* exon of *WNK1* cause hereditary sensory neuropathy type II. *J. Clin. Invest.* **118**, 2496–2505 (2008).
36. M. Shekarabi, R. G. Lafrenière, R. Gaudet, J. Laganière, M. M. Marcinkiewicz, P. A. Dion, G. A. Rouleau, Comparative analysis of the expression profile of *Wnk1* and *Wnk1/Hsn2* splice variants in developing and adult mouse tissues. *PLoS One* **8**, e57807 (2013).
37. W. M. Leiserson, E. W. Harkins, H. Keshishian, Fray, a *Drosophila* serine/threonine kinase homologous to mammalian PASK, is required for axonal ensheathment. *Neuron* **28**, 793–806 (2000).
38. A. C. Vitari, J. Thastrup, F. H. Rafiqi, M. Deak, N. A. Morrice, H. K. Karlsson, D. R. Alessi, Functional interactions of the SPAK/OSR1 kinases with their upstream activator WNK1 and downstream substrate NKCC1. *Biochem. J.* **397**, 223–231 (2006).
39. C. Pellegrino, O. Gubkina, M. Schaefer, H. Becq, A. Ludwig, M. Mukhtarov, I. Chudotvorova, S. Corby, Y. Salyha, S. Salozhin, P. Bregestovskii, I. Medina, Knocking down of the KCC2 in rat hippocampal neurons increases intracellular chloride concentration and compromises neuronal survival. *J. Physiol.* **589**, 2475–2496 (2011).
40. P. Friedel, P. Bregestovskii, I. Medina, Improved method for efficient imaging of intracellular Cl⁻ with Cl-Sensor using conventional fluorescence setup. *Front. Mol. Neurosci.* **6**, 7 (2013).
41. Y. Ben-Ari, J.-L. Gaiarsa, R. Tyzio, R. Khazipov, GABA: A pioneer transmitter that excites immature neurons and generates primitive oscillations. *Physiol. Rev.* **87**, 1215–1284 (2007).
42. J. A. Payne, Functional characterization of the neuronal-specific K-Cl cotransporter: Implications for [K⁺]_o regulation. *Am. J. Physiol.* **273**, C1516–C1525 (1997).
43. K. T. Kahle, N. D. Merner, P. Friedel, L. Silayeva, B. Liang, A. Khanna, Y. Shang, P. Lachance-Touchette, C. Bourassa, A. Levert, P. A. Dion, B. Walcott, D. Spiegelman, A. Dionne-Laporte, A. Hodgkinson, P. Awadalla, H. Nikbakht, J. Majewski, P. Cossette, T. Z. Deeb, S. J. Moss, I. Medina, G. A. Rouleau, Genetically encoded impairment of neuronal KCC2 cotransporter function in human idiopathic generalized epilepsy. *EMBO Rep.* **15**, 766–774 (2014).
44. N. T. Hertz, B. T. Wang, J. J. Allen, C. Zhang, A. C. Dar, A. L. Burlingame, K. M. Shokat, Chemical genetic approach for kinase-substrate mapping by covalent capture of thiophosphopeptides and analysis by mass spectrometry. *Curr. Protoc. Chem. Biol.* **2**, 15–36 (2010).
45. A. Bishop, O. Buzko, S. Heyeck-Dumas, I. Jung, B. Kraybill, Y. Liu, K. Shah, S. Ulrich, L. Witucki, F. Yang, C. Zhang, K. M. Shokat, Unnatural ligands for engineered proteins: New tools for chemical genetics. *Annu. Rev. Biophys. Biomol. Struct.* **29**, 577–606 (2000).
46. A. C. Bishop, J. A. Ubersax, D. T. Petsch, D. P. Matheos, N. S. Gray, J. Blethrow, E. Shimizu, J. Z. Tsien, P. G. Schultz, M. D. Rose, J. L. Wood, D. O. Morgan, K. M. Shokat, A chemical switch for inhibitor-sensitive alleles of any protein kinase. *Nature* **407**, 395–401 (2000).
47. P. Uvarov, A. Ludwig, M. Markkanen, P. Pruunsild, K. Kaila, E. Delpire, T. Timmusk, C. Rivera, M. S. Airaksinen, A novel N-terminal isoform of the neuron-specific K-Cl cotransporter KCC2. *J. Biol. Chem.* **282**, 30570–30576 (2007).
48. K. Piechotta, J. Lu, E. Delpire, Cation chloride cotransporters interact with the stress-related kinases Ste20-related proline-alanine-rich kinase (SPAK) and oxidative stress response 1 (OSR1). *J. Biol. Chem.* **277**, 50812–50819 (2002).
49. N.-S. Woo, J. Lu, R. England, R. McClellan, S. Dufour, D. B. Mount, A. Y. Deutch, D. M. Lovinger, E. Delpire, Hyperexcitability and epilepsy associated with disruption of the mouse neuronal-specific K–Cl cotransporter gene. *Hippocampus* **12**, 258–268 (2002).
50. L. Zhu, D. Lovinger, E. Delpire, Cortical neurons lacking KCC2 expression show impaired regulation of intracellular chloride. *J. Neurophysiol.* **93**, 1557–1568 (2005).
51. P. Uvarov, O. Llano, A. Ludwig, M. S. Airaksinen, C. Rivera, in *Cellular Migration and Formation of Neuronal Connections*, J. L. R. R. Rakic, Ed. (Academic Press, Oxford, 2013), pp. 975–998.
52. I. Medina, P. Friedel, C. Rivera, K. T. Kahle, N. Kourdougli, P. Uvarov, C. Pellegrino, Current view on the functional regulation of the neuronal K⁺-Cl⁻ cotransporter KCC2. *Front. Cell. Neurosci.* **8**, 27 (2014).
53. K. Ganguly, A. F. Schinder, S. T. Wong, M. Poo, GABA itself promotes the developmental switch of neuronal GABAergic responses from excitation to inhibition. *Cell* **105**, 521–532 (2001).
54. E. Leitch, J. Coaker, C. Young, V. Mehta, E. Semagor, GABA type-A activity controls its own developmental polarity switch in the maturing retina. *J. Neurosci.* **25**, 4801–4805 (2005).
55. S. Shibata, Y. Kakazu, A. Okabe, A. Fukuda, J. Nabekura, Experience-dependent changes in intracellular Cl⁻ regulation in developing auditory neurons. *Neurosci. Res.* **48**, 211–220 (2004).

56. A. C. Bishop, O. Buzko, K. M. Shokat, Magic bullets for protein kinases. *Trends Cell Biol.* **11**, 167–172 (2001).
57. B. P. Zambrowicz, A. Abuin, R. Ramirez-Solis, L. J. Richter, J. Piggott, H. BeltrandelRio, E. C. Buxton, J. Edwards, R. A. Finch, C. J. Friddle, A. Gupta, G. Hansen, Y. Hu, W. Huang, C. Jaing, B. W. Key Jr., P. Kipp, B. Kohlhauff, Z.-Q. Ma, D. Markesich, R. Payne, D. G. Potter, N. Qian, J. Shaw, J. Schrick, Z.-Z. Shi, M. J. Sparks, I. Van Sligtenhorst, P. Vogel, W. Walke, N. Xu, Q. Zhu, C. Person, A. T. Sands, Wnk1 kinase deficiency lowers blood pressure in mice: A gene-trap screen to identify potential targets for therapeutic intervention. *Proc. Natl. Acad. Sci. U.S.A.* **100**, 14109–14114 (2003).
58. R. Tyzio, R. Nardou, D. C. Ferrari, T. Tsintsadze, A. Shahrokhi, S. Eftekhari, I. Khalilov, V. Tsintsadze, C. Brouchoud, G. Chazal, E. Lemonnier, N. Lozovaya, N. Burnashev, Y. Ben-Ari, Oxytocin-mediated GABA inhibition during delivery attenuates autism pathogenesis in rodent offspring. *Science* **343**, 675–679 (2014).
59. V. I. Dzhalal, D. M. Talos, D. A. Scrulla, A. C. Brumback, G. C. Mathews, T. A. Benke, E. Delpire, F. E. Jensen, K. J. Staley, NKCC1 transporter facilitates seizures in the developing brain. *Nat. Med.* **11**, 1205–1213 (2005).
60. R. Miles, P. Blaesse, G. Huberfeld, L. Wittner, K. Kaila, in *Jasper's Basic Mechanisms of the Epilepsies*, J. L. Noebels, M. Avoli, M. A. Rogawski, R. W. Olsen, A. V. Delgado-Escueta, Eds. (National Center for Biotechnology Information, Bethesda, MD, 2012).
61. J. A. Coull, D. Boudreau, K. Bachand, S. A. Prescott, F. Nault, A. Sök, P. De Koninck, Y. De Koninck, Trans-synaptic shift in anion gradient in spinal lamina I neurons as a mechanism of neuropathic pain. *Nature* **424**, 938–942 (2003).
62. M. Puskarjov, P. Seja, S. E. Heron, T. C. Williams, F. Ahmad, X. Iona, K. L. Oliver, B. E. Grinton, L. Vutskits, I. E. Scheffer, S. Petrou, P. Blaesse, L. M. Dibbens, S. F. Berkovic, K. Kaila, A variant of KCC2 from patients with febrile seizures impairs neuronal Cl⁻ extrusion and dendritic spine formation. *EMBO Rep.* **15**, 723–729 (2014).
63. V. Bercier, E. Brustein, M. Liao, P. A. Dion, R. G. Lafrenière, G. A. Rouleau, P. Drapeau, WNK1/HSN2 mutation in human peripheral neuropathy deregulates KCC2 expression and posterior lateral line development in zebrafish (*Danio rerio*). *PLoS Genet.* **9**, e1003124 (2013).
64. T. Waseem, M. Mukhtarov, S. Buldakova, I. Medina, P. Bregestovski, Genetically encoded Cl⁻-Sensor as a tool for monitoring of Cl⁻-dependent processes in small neuronal compartments. *J. Neurosci. Methods* **193**, 14–23 (2010).
65. J. Luo, M. J. Emanuele, D. Li, C. J. Creighton, M. R. Schlabach, T. F. Westbrook, K.-K. Wong, S. J. Elledge, A genome-wide RNAi screen identifies multiple synthetic lethal interactions with the Ras oncogene. *Cell* **137**, 835–848 (2009).
66. T. Buerli, C. Pellegrino, K. Baer, B. Lardi-Studler, I. Chudotvorova, J.-M. Fritschy, I. Medina, C. Fuhrer, Efficient transfection of DNA or shRNA vectors into neurons using magnetofection. *Nat. Protoc.* **2**, 3090–3101 (2007).
67. I. Chudotvorova, A. Ivanov, S. Rama, C. A. Hübner, C. Pellegrino, Y. Ben-Ari, I. Medina, Early expression of KCC2 in rat hippocampal cultures augments expression of functional GABA synapses. *J. Physiol.* **566**, 671–679 (2005).
68. R. Tyzio, G. L. Holmes, Y. Ben-Ari, R. Khazipov, Timing of the developmental switch in GABA_A mediated signaling from excitation to inhibition in CA3 rat hippocampus using gramicidin perforated patch and extracellular recordings. *Epilepsia* **48**, 96–105 (2007).
69. R. Tyzio, A. Ivanov, C. Bernard, G. L. Holmes, Y. Ben-Ari, R. Khazipov, Membrane potential of CA3 hippocampal pyramidal cells during postnatal development. *J. Neurophysiol.* **90**, 2964–2972 (2003).
70. A. Carabalona, S. Beguin, E. Pallesi-Pocachard, E. Buhler, C. Pellegrino, K. Arnaud, P. Hubert, M. Oualha, J. P. Siffroi, S. Khantane, I. Coupry, C. Goizet, A. B. Gelot, A. Represa, C. Cardoso, A glial origin for periventricular nodular heterotopia caused by impaired expression of Filamin-A. *Hum. Mol. Genet.* **21**, 1004–1017 (2012).
71. C. Zhang, D. M. Kenski, J. L. Paulson, A. Bonshien, G. Sessa, J. V. Cross, D. J. Templeton, K. M. Shokat, A second-site suppressor strategy for chemical genetic analysis of diverse protein kinases. *Nat. Methods* **2**, 435–441 (2005).

Acknowledgments: We are grateful to Y. Ben-Ari (Neurochlore) and D. Clapham (Harvard) for critical reading of and valuable comments on the manuscript; G. Chazal and N. Ferrand for help at the initial stages of the work; F. Bader for animal care and assistance in in utero electroporation surgery; J. Guyot for blind analysis of KCC2 clusters; and C. Rivera for providing pcDNA encoding HA-KCC2. **Funding:** This work was supported by a French National Research Agency [L'Agence nationale de la recherche (ANR)] grant to I.M.; an INSERM-CR-PACA-FEDER grant to P.F.; and a Harvard–Massachusetts Institute of Technology Award in Neuroscience Grant and the Manton Center for Orphan Diseases at Harvard University and Boston Children's Hospital grant to K.T.K. **Author contributions:** K.T.K., K.M.S., and I.M. conceived and designed the experiments. P.F., K.T.K., J.Z., N.H., L.I.P., E.B., F.S., J.D., A.R.K., and P.N.B. performed the experiments. P.F., K.T.K., J.Z., N.H., L.P., and I.M. analyzed the data. J.D. and P.N.B. provided samples. K.T.K. and I.M. wrote the manuscript. **Competing interests:** The authors declare that they have no competing interests. **Data and materials availability:** Princeton University holds patents on the analog-sensitive kinase technology; however, all constructs and antibodies that were used in this work are available on request.

Submitted 8 October 2014

Accepted 11 June 2015

Final Publication 30 June 2015

10.1126/scisignal.aaa0354

Citation: P. Friedel, K. T. Kahle, J. Zhang, N. Hertz, L. I. Pisella, E. Buhler, F. Schaller, J. Duan, A. R. Khanna, P. N. Bishop, K. M. Shokat, I. Medina, WNK1-regulated inhibitory phosphorylation of the KCC2 cotransporter maintains the depolarizing action of GABA in immature neurons. *Sci. Signal.* **8**, ra65 (2015).

WNK1-regulated inhibitory phosphorylation of the KCC2 cotransporter maintains the depolarizing action of GABA in immature neurons

Perrine Friedel, Kristopher T. Kahle, Jinwei Zhang, Nicholas Hertz, Lucie I. Pisella, Emmanuelle Buhler, Fabienne Schaller, JingJing Duan, Arjun R. Khanna, Paul N. Bishop, Kevan M. Shokat and Igor Medina

Sci. Signal. **8** (383), ra65.
DOI: 10.1126/scisignal.aaa0354

Keeping immature neurons excited

After birth, signaling by the neurotransmitter GABA in the brain switches from excitatory to inhibitory. GABA mediates both the excitatory and inhibitory responses by binding to ligand-gated ion channels that conduct Cl⁻. Whether opening these channels triggers hyperpolarization (inhibition) or depolarization (excitation) depends on the concentration of Cl⁻ in neurons. Friedel *et al.* identified phosphorylation events in the K⁺-Cl⁻ cotransporter KCC2, which depended on the activity of the kinase WNK1, inhibited KCC2 activity, and contributed to the depolarizing effect of GABA-mediated signaling in immature rat neurons by maintaining high internal Cl⁻ concentration. This regulatory mechanism has implications for the normal developmental excitatory-to-inhibitory GABA switch and neurodevelopmental diseases, such as autism, epilepsy, and spasticity.

ARTICLE TOOLS

<http://stke.sciencemag.org/content/8/383/ra65>

SUPPLEMENTARY MATERIALS

<http://stke.sciencemag.org/content/suppl/2015/06/26/8.383.ra65.DC1>

RELATED CONTENT

<http://stm.sciencemag.org/content/scitransmed/6/244/244ra89.full>
<http://stke.sciencemag.org/content/sigtrans/7/334/re3.full>
<http://stke.sciencemag.org/content/sigtrans/7/324/ra41.full>
<http://stke.sciencemag.org/content/sigtrans/8/376/ec121.abstract>
<http://stke.sciencemag.org/content/sigtrans/3/152/re10.full>
<http://stke.sciencemag.org/content/sigtrans/8/383/pc16.full>
<http://stke.sciencemag.org/content/sigtrans/9/439/ra77.full>
<http://stke.sciencemag.org/content/sigtrans/9/444/ec207.abstract>
<http://science.sciencemag.org/content/sci/353/6303/1037.full>

REFERENCES

This article cites 69 articles, 16 of which you can access for free
<http://stke.sciencemag.org/content/8/383/ra65#BIBL>

PERMISSIONS

<http://www.sciencemag.org/help/reprints-and-permissions>

Use of this article is subject to the [Terms of Service](#)